

Memo – Comments on SSM’s review of SKB’s earthquake modelling

Harald Hökmark

Billy Fälth

Clay Technology AB

Raymond Munier

Diego Mas Ivars

SKB

December 2015.

Contents

1	Introduktion.....	3
1.1	Kommentarer till SSMs granskningsutlåtande	3
1.1.1	Respektavstånd	3
1.1.2	Överförenklade modeller	3
1.1.3	Mindre zoner	4
1.1.4	Stokastiska målsprickor	6
1.1.5	Skjuvrörelser.....	7
2	SKB's assessment of the earthquake scenario	9
2.1	General	9
2.2	Dynamic 3DEC simulations conducted for the SR-Site safety assessment.....	9
2.3	Benchmarking	10
2.4	Additional applications of the simulation method	10
2.5	Ongoing and planned work	13
2.6	Perspectives on the degree of conservativeness	14
2.6.1	Magnitude overestimate.....	15
2.6.2	Planarity of target fractures	18
2.6.3	Representation of fault edges.....	19
2.7	3DEC simulation method – summary	20
3	Comments on the modelling results in Yoon et al. (2014)	22
3.1	Problems associated with the of 2D approach.....	22
3.1.1	Slip of individual fractures.....	22
3.1.2	Fracture interaction and plastic deformations	23
3.1.3	Thermal loads.....	24
3.1.4	Seismic loads	29
3.2	Impact and handling of “outliers”	29
3.3	Unrealistic results	30
3.3.1	Relation between fracture size and fracture shear displacement.....	30
3.3.2	Fault size and fault slip	32
3.3.3	Fault slip velocities	34
3.4	Possible explanations for the PFC results.....	35
3.4.1	Smooth-joint representation of discontinuities (faults, fractures, joints, foliation planes)	35
3.4.2	Calibration of smooth joint mechanical properties	37
3.4.3	Smooth joint based DFN (effect of discontinuity intersections and discontinuity terminations).....	41
3.4.4	Type of bond used vs. rock behaviour modelling and rock damage estimation	44
3.5	Final remarks	44
3.5.1	General	44
3.5.2	Two dimensional model approach.....	46
3.5.3	Handling of “Outliers”	47
3.5.4	Unrealistic results.....	47
4	Conclusions.....	49
5	References	50

1 Introduktion

Denna PM är en respons på de delar av SSMs granskningsutlåtande (SSM 2015) som rör seismiskt inducerade sprickrörelser i förvaret. I det följande presenteras i Avsnitt 1 kommentarer från SKB om SSM:s preliminära granskningsutlåtande. Som stöd i argumentationen ges i Avsnitt 2 en sammanfattning av SKB:s modelleringsmetod i SR-Site samt resultat från därefter utförda beräkningar, vilka visar på konservatismen i SKB:s beräkningsmetod och som därmed understöder slutsatserna i SR-Site. Vidare refereras till Avsnitt 3, som innehåller kommentarer till SSM Technical note 2014:59 (Yoon et al. 2014).

1.1 Kommentarer till SSMs granskningsutlåtande

1.1.1 Respektavstånd

(SSM 2015, s 74): "SSM anser därför att "respektavståndet" bör ökas jämfört med 100 m om osäkerheterna för placering samt den interna strukturen hos deformationszonerna inte kan minskas genom detaljundersökningar som genomförs under en eventuell uppförandefas (se även SSM Technical note 2014:07)."

Som en kommentar till ovanstående vill SKB framhålla att det är nödvändigt att särskilja respektavstånd, vilket är kopplat till seismisk risk, ifrån geometrisk osäkerhet vilken är kopplad till platsmodellen och kan hanteras med andra medel (se tex Munier et al. 2003, avsnitt 6.3). Oavsett var zonen skär förvarsdjupet kommer respektavståndet vara detsamma, med förbehållet att nya analysresultat inte ändrar dess storlek. Den geometriska osäkerheten förväntas minska i takt med att vi får mer information ifrån de detaljerade platsundersökningarna. Den kvarstående geometriska osäkerheten kommer att adderas till respektavståndet.

(SSM 2015, s 55): "SSM:s externa experter föreslår ett utökat "respektavstånd" från zoner längre än tre kilometer (SSM Technical note 2014:07) för att ta höjd för osäkerheterna i den nuvarande deformationszonsmodellen för Forsmark (SKB TR-08-05)."

I avsnitt 2.6 visar vi att säkerhetsmarginalerna i våra beräkningar är sådana att de respektavstånd som nu gäller snarare är alltför väl tilltagna och kommenterar också i det avsnittet respektavstånd till mindre zoner. Se också text nedan under "överförenklade modeller".

1.1.2 Överförenklade modeller

(SSM 2015, s 55): "Den nuvarande stiliserade modellen med en plan rektangulär deformationszon kan anses vara överförenklad. Överförenklingen gäller inte bara enstaka deformationszoners strykning, stupning eller ytform, men även deformationszonernas terminationer, skärningar och geometriska förhållande till varandra och till bergspänningstillståndet."

"...Det bör därför vara möjligt att undersöka särskilda fenomen som beror på ytråhet och vågighet hos sprickorna och som kan påverka bedömningen av jordskalvens inverkan."

SKB har sedan förberedelserna för säkerhetsanalysen SR-Can tillämpat en medveten strategi med avsikt att renodla problemställningarna (Fälth and Hökmark 2006b; Fälth et al. 2007, 2008). Som ett led i detta har vi avsiktligt anammat en metodik som går ut på att använda förenklade geometrier

och stegvist ökad komplexitet i modelleringen, för att modellera gränssättande, konservativa fall då detta underlättar förståelse av den mekaniska processen, och av modelleringsverktygets möjligheter och begränsningar. Relevansen av detta synsätt tycks delas av SSM:s experter Ofoegbu and Smart (2012):

“SwRI-CNWRA kom fram till att SKB:s analys är ändamålsenlig för att bedöma jordbävningsinducerade skjuvdeformationer eftersom (i) analysen utfördes med hjälp av en väletablerad datakod (3DEC) för modellering av mekaniska förändringar i en sprickig bergmassa; (ii) en meningsfull spridning på parametervärden användes i modelleringen, som till exempel geometrin på förkastningar och sprickor, mekaniska egenskaper samt magnitud och riktning på in-situ-spänningar; och (iii) tillvägagångssättet för att initiera och propagera förkastningsrörelse var konsistent med de förmodade mekaniska förändringar som förknippas med dynamisk förkastningsrörelse.”

I Avsnitt 2.6 visar vi några exempel på hur de förenklade beskrivningarna av förkastningsplanens geometri, brottets utbredning över förkastningsplanet och brottets terminering vid förkastningsplanets kanter leder till överskattningar av jordskalvets magnitud och överskattningar av de spänningskoncentrationer som utbildas vid förkastningsplanets kanter. Vi visar också att mer realistiska beskrivningar leder till drastiskt reducerade sekundärrörelser. Det är för övrigt inte bara primärzonen och processerna i primärzonen som är medvetet förenklade. Även beskrivningen av det omgivande berget och de stora sprickor som potentiellt skulle kunna skjuvas med stora belopp är medvetet grovt förenklade. De stora sprickorna antas vara omgivna av ett elastiskt kontinuum, vilket innebär att ingen töjningsenergi förbrukas på, t ex, friktionsarbete i omgivningen. I Avsnitt 2.6 visar vi att denna förenkling bidrar till att överdriva sekundärrörelserna. På samma sätt visar vi exempel på hur en blygsam störning av en sprickas planaritet kan reducera den inducerade rörelsen kraftigt. Vi håller alltså med om att våra modeller är överförenklade, vilket innebär att det i den sammantagna hanteringen av jordsskalvsscenarioet finns stora säkerhetsmarginaler. Mer realistiska antaganden beträffande alla de förhållanden som beskrivs i Avsnitt 2.6 skulle kunna ge försumbara sekundärrörelser.

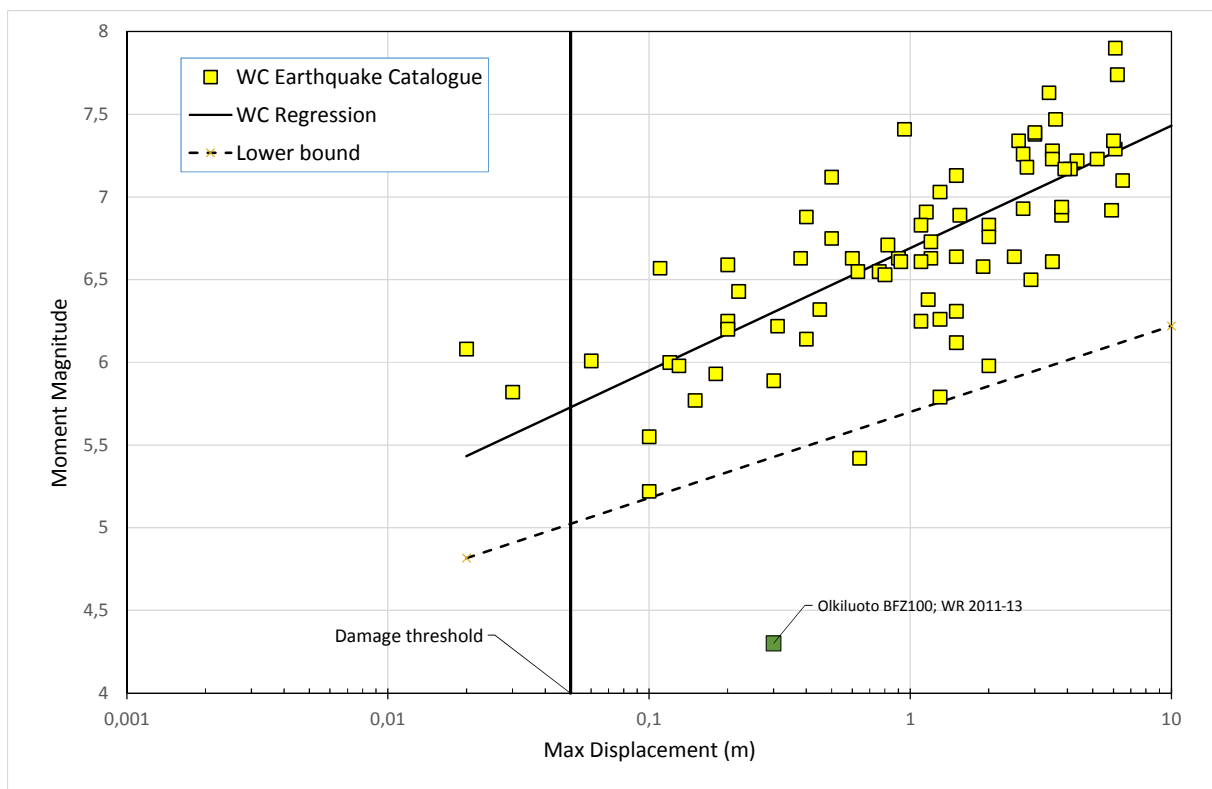
SKB anser i likhet med SSM att alternativa modelleringsangrepp kan stärka förtroendet för modelleringsansatserna och de slutsatser som kan dras ur dessa. Man skulle kanske också kunna finna vägar att rättfärdiga en något mindre överdriven konservatism och på så sätt reducera den beräknade seismiska risken. Modelleringen som utförts av SSM:s experter (Yoon et al. 2014) visar emellertid tydligt på utmaningarna att dra relevanta slutsatser ur alltför komplext uppbyggda modeller där komplexiteten dessutom införts på bekostnad av den nödvändiga 3-dimensionella representationen av spricknätverket och spänningsvariationerna.

1.1.3 Mindre zoner

(SSM 2015, s 55): “SKB tar dessutom inte hänsyn till de lokala mindre deformationszonerna med en längd mellan en och tre kilometer. Dessa lokala deformationszoner bestämmer slutförvarets detaljerade layout och, förutom att kunna påverka effekten av ett jordskalv som inträffar på en annan längre deformationszon, kan de också hysa mindre jordskalv som ligger närmare deponeringspositionerna i och med att de lokala deformationszonerna inte är försedda med ”respektavstånd”.

Regressionssamband mellan momentmagnituder och maximala primärrörelser på deformationszoner ger att 50 mm maximal primärrörelse svarar mot skalv av momentmagnituder runt Mw 5.75 (Figur

1-1). Spridningen i magnituddata är dock stor: i figuren har vi lagt in en rät linje, "Lower bound", som, om man extrapolerar till 50 mm maxrörelse, visar att det fordras skalv av minst magnitud Mw 5.0 för att den maximala primärrörelsen skall bli 50 mm eller mer. La Pointe et al. (1997) hävdar att extrapolationer av regressionssambanden till små magnituder tenderar att överskatta den maximala rörelsen, detta med hänvisning till styvhetskillnader mellan stora och små deformationszoner. Sammanfattningsvis bör skalv av magnitud 5.0 och mindre inte kunna ge primärrörelser större än 50 mm och därmed inte heller sekundärrörelser större än 50 mm, oavsett avstånd. Således krävs inga respektavstånd till dessa zoner. Däremot måste naturligtvis själva zonen, och dess "damage zone" (ingår i definitionen av tjocklek) undvikas i deponeringshål.



Figur 1-1. Momentmagnitud som funktion av maximal primärrörelse (Wells and Coppersmith 1994). För att primärrörelsen skall bli 50 mm eller mer fordras, enligt regressionen, en momentmagnitud av Mw 5.75. En undre gräns, baserad på "Lower bound"-linjen, är Mw 5.0. I figuren visas också exempel på ett syntetisk 3DEC skalv med mycket starkt överdriven primärrörelse på en liten deformationszon, se text nedan.

I alla de beräkningar som gjorts till dags dato har i själva verket den största sekundära sprickrörelsen, också på de minsta avstånden, inte i något fall utgjort mer än ca 10 procent av primärrörelsen. Detta gäller också för de enstaka modelleringsfall som analyserats med målsprickor som skärs av primärzonen, se Figur 3-17 och 3-18 i (Fälth and Hökmark 2011) och Figur 4-20 i (Fälth and Hökmark 2006b). Också givet de osäkerheter som nödvändigtvis finns i beräkningsresultat som tagits fram för mycket små avstånd illustrerar dessa exempel att den största maximala primärrörelsen rimligen måste vara väsentligt större än 50 mm för att ett respektavstånd skall behövas, och att det därför finns betydande marginaler i respektavståndsregeln. Följer man "Lower bound" linjen i Figur 1-1, vilket är konservativt, och antar att sekundärrörelsen är 10 procent av primärrörelsen finner man att

skalvet måste ha en magnitud av Mw 5.5, vilket svarar mot en "rupture area" av ca 20 km² enligt Leonards regression och ännu mer enligt Wells-Coppersmiths regression (Figure 2-1). Beaktar man dessutom att "rupture area" inte nödvändigtvis måste sammanfalla med deformationszonens area (Figure 2-2) inser man att det finns marginaler också i dessa uppskattningar och att det inte är nödvändigt med respektavstånd kring mindre deformationszoner.

Skrivningen här baseras på en kombination av konservativt tolkade empiriska data och på beräkningsresultat som erhållits med beräkningstekniken som beskrivs i Kapitel 2, se också text under "Överförenklade modeller" ovan. Observera dock att det finns exempel på beräkningsresultat som ger sekundära förskjutningar i storleksordningen 30 mm (sprickdiameter 150 m) på 100 m avstånd från skalv som modelleras på mindre deformationszoner (Fälth and Hökmark 2011, 2012). I dessa fall är alla överförenklingar schematiskt applicerade fullt ut utan koppling till de empiriska rörelse-magnitudsambanden i Figur 1-1. Till exempel har ett skalv med Mw 4.3 och maximal primärrörelse på 0.3 m simulerats, vilket är mycket extremt (Olkiluoto BFZ100 i Figur 1-1). Eftersom zonen är mycket liten (0.9 km²) bidrog även effekten av närliggande skarpa kanter till de starkt överdrivna sekundärrörelserna (maximum ca 30 mm, också för spricka som skär genom deformationszonen).

1.1.4 Stokastiska målsprickor

(SSM 2015, s 55): "SSM anser också att SKB bör utveckla mera realistiska spricknätverk av sekundära sprickor för sina jordskalvssimuleringar. Som underlag för hittills genomförda simuleringar har SKB använt en tredimensionell representation med sekundära sprickor varav samtliga med diametrar på 300 m och standardiserade orienteringar. En begränsning med denna metod är att det inte är möjligt att belysa effekten av variationen hos sprickorienteringarna och sprickstorlekarna..."

"...En annan begränsning är, liksom för SKB:s modeller av deformationszoner, att effekten av spricknätverket med sprickornas skärningar med varandra och med deformationszonerna inte kan studeras i detalj..."

Vi visar i avsnitt 2.6 att spricknätverk kring målsprickorna tenderar att minska de sekundära rörelserna. Det är således konservativt att inte inkludera någon DFN i jordskalvsmodelleringarna. Vi avser emellertid komplettera våra försök med fler fall för att bättre kvantifiera den avskärmande effekten. Med detta önskar vi nå större förståelse för de mest relevanta processerna samt en möjlighet att på ett trovärdigt sätt tillämpa mindre konservativa antaganden i kommande säkerhetsanalyser.

Sprickor av olika storlek adresseras i våra modeller med hjälp av skalning. För detta krävs ett grundantagande om berget som elastiskt medium, som en första ordningens approximation, och att Eshelbys ekvationer (Eshelby 1957) är giltiga. Vi har hittills inte tagit del av övertygande argumentation som på ett avgörande vis kan utmana dessa antaganden.

Fälth (2015) gjorde simuleringar baserade på Forsmarkdata där sekundärrörelser på målsprickor med 300 m diameter beräknades. Rörelserna beräknades för ett flertal (22 stycken) sprickorienteringar, både generiska orienteringar och orienteringar baserade på platsdata. Ingen sprickrörelse överskred 50 mm inom området för det planerade förvaret. Variationen i sprickorientering täcker i praktiken in den variation som en DFN skulle ge.

1.1.5 Skjuvrörelser

(SSM 2015, s 52): "SSM bedömer att betydande ytterligare insatser erfordras innan en eventuell provdrift av slutförvarsanläggningen kan bli aktuell. SSM:s oberoende beräkningar av skjuvrörelser orsakade av pre- och post-glaciala jordskalv överensstämmer överlag med SKB:s resultat men vissa skillnader kan ändå observeras (se även avsnitt 4.16, 5.17, 6.2 ännu ej publicerade; SSM Technical note 2014:59):

- sambandet mellan sprickans skjuvrörelse och sprickans storlek verkar inte gälla i samtliga fall
- sekundära sprickor uppvisar ett bredare variationsintervall för skjuvrörelser än det som redovisas av SKB
- måttliga jordskalv (dvs. med momentmagnitud ca 4) på mindre deformationszoner inom deponeringsområdena kan i vissa fall inducera skjuvrörelser större än 50 mm i sekundära korta sprickor"

Dessa resultat antyder att SKB:s koncept med "kritiska sprickor" och "respektavstånd" inte är helt tillförlitliga och exkluderande i en deterministisk mening."

(SSM 2015, s 56): "Enligt SSM:s bedömning ger dessa simuleringar relevanta resultat trots att dessa spricknätverk är tvådimensionella och inte tredimensionella som SKB:s."

(SSM 2015, s 73): "Beträffande val av områden för placering av deponeringsområden har SSM låtit genomföra egna beräkningar avseende sekundära sprickors rörelser och kommit fram till att varken ett "respektavstånd" på 100 m från en seismisk aktiv deformationszon eller en sprickdiameter mindre än 125 m helt utesluter sekundära rörelser större än 50 mm (SSM Technical note 2014:59; SSM Technical note Geomecon/sprickor)."

Sprickrörelsen beror inte endast på sprickans storlek, utan även på dess orientering relativt spänningsfältet (stabilitet) och på dess position relativt primärzonen (dvs. belastningen den utsätts för). Detta innebär att en mindre spricka med liten stabilitetsmarginal, vilken är placerad nära primärzonen kan röra sig lika mycket som en större stabil spricka på ett större avstånd från zonen. Dock är det så, att för en given sprickorientering och given belastning skalar rörelsen med storleken. Detta visas av Fälth et al. (2010). Notera att skalningen gäller för stora rörelser då hela sprickytan är engagerad. Små rörelser skalar inte nödvändigtvis med sprickstorleken, men dessa rörelser är ändå betydelselösa.

Vi visar i Avsnitt 3 att 2D-modeller inte ger användbara resultat i detta sammanhang eftersom detta i första hand är ett 3D-problem. En 2D-modell överdriver kraftigt sprickrörelserna och de åtföljande spänningskoncentrationerna runt sprickkanterna. Vidare krävs en 3D-modell för att på ett korrekt sätt beräkna sprickornas stabilitet och för att propagera seismiska vågor korrekt. Dessutom visas i Avsnitt 3.1.3 att 2D-modellering av en termo-mekanisk utveckling med spänningsreduktion under uppvärmning inte ger resultat relevanta för ett verkligt tredimensionellt fall. Detta indikerar att modelleringen av Yoon et al. (2014) inte simulerar de grundläggande mekaniska processerna korrekt, och därmed också att de simulerade sprickrörelserna kan ifrågasättas.

Extrapolering av data från verkliga skalv (Figur 1-1) pekar på maximala primärrörelser i storleksordningen 1 mm för M4 skalv. Även givet en betydande osäkerhetsmarginal i extrapolationen kan man utesluta sekundära rörelser på 50 mm för så små skalv. Notera det extrema beräkningsfallet redovisat under rubriken "Mindre zoner" ovan där ett M4.3 skalv med 300 mm maxrörelse

simulerades (Fälth and Hökmark 2011, 2012). Detta extrema fall gav på 100 m avstånd 30 mm sekundärrörelse på en spricka med 150 m diameter.

2 SKB's assessment of the earthquake scenario

2.1 General

The seismic impact on the nuclear waste repository that is of potential importance to the long-term safety has been concluded to be that of shear displacements along rock fractures that intersect canister positions (Fälth et al. 2010). Canisters sheared 50 mm or more count as damaged based on results in Raiko et al. (2010). Consequently, canister positions intersected by fractures or fracture zones large enough to host earthquakes that, according to established relations between rupture area and fault displacement, could slip by 50 mm or more, are rejected. It cannot, however, be ruled out that large secondary shear displacements could be induced on smaller, optimally oriented, fractures that intersect canister positions located at some distance from a large, potentially seismically active, deformation zone.

In the following, we provide a brief summary of the modelling efforts conducted in the safety assessment SR-Site and in subsequent efforts.

2.2 Dynamic 3DEC simulations conducted for the SR-Site safety assessment

The dynamic 3DEC simulations referred to in SR-Site are those reported by Fälth et al. (2010). The modelling approach can briefly be described as follows:

- Earthquakes were simulated on schematic, hypothetical, rectangular deformation zones (primary faults) without couplings to the Forsmark site or to any other site.
- The area of the primary faults ranged between 10 and 1000 km³. In all cases analysed, the entire fault area was ruptured, meaning that the rupture area was always identical with the fault area. Moment magnitudes ranged between Mw 5 and Mw 7. In all cases the moment magnitude was higher than the magnitude that would be typical of the rupture area as inferred from database regressions established by Wells and Coppersmith (1994) and Leonard (2010).
- Stress fields were schematically defined without couplings to any site. Stress magnitudes were set just high enough to power earthquakes of the magnitudes described above. Principal stress orientations were set to give reverse faulting stress regimes.
- The rupture was initiated at the centre of the fault and programmed to propagate outwardly along the fault plane with a velocity corresponding a specified fraction (typically 70%) of the shear wave velocity of the surrounding elastic medium.
- The rupture process was programmed as a controlled strength breakdown: as soon as the rupture front arrived at a point on the fault plane, the strength at that point was ramped down over a specified time interval (typically 0.5 seconds).

- The response of the rock mass to the stress waves and the stress redistribution caused by the rupture and the associated slip on the primary fault was monitored and recorded in terms of shear displacements on differently oriented 300 m diameter perfectly planar fractures explicitly modelled at different distances from the primary fault

2.3 Benchmarking

The dynamic logic of the 3DEC code has been extensively tested and verified for cases where typical seismic loads, compatible with plane waves and generated by distant sources, have been applied to the boundaries of models containing the structure under study (ITASCA 2013). In models relevant for assessing the seismic risk for the nuclear waste repository, however, it must be possible to represent the seismic source explicitly within the model volume. For benchmarking of the simulation method a specific 3DEC model, with a primary fault programmed to rupture as described above for the SR-Site simulations, was examined for waveforms at a number of points at different positions and distances from the primary fault (Fälth 2015). Waveform results, obtained from a corresponding Compsyn model (Spudich and Xu 2002) programmed to produce the same temporal and spatial development of the rupture, were compared with the 3DEC wave forms. The agreement between the two sets of result was very satisfactory, meaning that the 3DEC dynamic logic should be considered adequate for the type of simulations conducted for the SR-Site assessment of the seismic risk.

2.4 Additional applications of the simulation method

Since the completion of the simulations referred to in the SR-Site reports, a number of additional simulations have been conducted, however with less schematic assumptions regarding, particularly, the fault geometry, the stress field and the fault strength breakdown. Simulations have been conducted both for SKB (Fälth and Hökmark 2013; Fälth 2015) and for Posiva (Fälth and Hökmark 2011, 2012, 2015).

In the SKB models, the initial stresses were based on the Forsmark most likely stress model (Martin 2007; SKB 2008). Simulations were conducted for end-glacial stress conditions (Fälth 2015) with glacial stress additions obtained from Lund et al. (2009) and for thermal stress conditions prevailing 100 and 1000 years after deposition (Fälth and Hökmark 2013). As shown in Fälth and Hökmark (2013), gently dipping Forsmark deformation zones, such as ZFMA2, are significantly less stable than steeply dipping ones at depths down to a couple of kilometres. Additionally, gently dipping deformation zones will be further destabilized under end-glacial conditions, i.e., during time periods known to have exhibited increased seismic activity, with large earthquakes in the otherwise stable Baltic Shield, in the past. Steeply dipping zones, in contrast, will be further stabilized under end-glacial conditions. ZFMA2 is the only large gently dipping deformation zone identified at the Forsmark site. Both modelling and measurements indicate that stress release, resulting in lower horizontal stress magnitudes above ZFMA2, has occurred (Martin 2007; SKB 2008). This suggests that ZFMA2 may be close to the stability limit over significant portions of its fault area, and that it, consequently (in contrast to the many steeply dipping zones) is reasonably likely to host large earthquakes.

The Posiva models were analysed for end-glacial conditions (Fälth and Hökmark 2011, 2012) and for present-day stress conditions (Fälth and Hökmark 2015).

It is beyond the scope of this PM to go into the details of these simulations. The following should however be noted:

- In all models, the resulting moment magnitudes plot above the area-magnitude regressions established by Wells and Coppersmith (1994) and Leonard (2010), cf. Figure 2-1 below. Given that the rupture area equals the fault area in all 3DEC cases, this means that the strain energy release was considerably overestimated compared to the strain energy release that would be realistic for real faults of these sizes, i.e., for faults where only the most unstable portions of the fault plane would rupture. There are no data on how much larger the fault areas of the catalogue earthquakes are than the rupture areas given in the studied catalogues (Wells and Coppersmith 1994; Leonard 2010). If the fault areas would be twice the rupture area, as assumed in Figure 2-2, the magnitude exaggeration in the 3DEC simulations made for Forsmark and Olkiluoto would obviously be very significant.
- In all models, the rupture was abruptly arrested at the fault edges. The largest secondary fracture displacements in our models are caused by stress concentrations around unrealistically sharp fault edges.
- In all models, the target fractures were, as in the SR-Site calculations, perfectly planar.
- In contrast to the SR-Site simulations, numerous target fracture orientations were tried in order to ensure that the largest induced displacements would be captured.
- In all models the target fractures were located distant enough from each other that fracture-fracture interactions were negligible, i.e., all secondary displacements found among the target fractures would be, with good approximation, equivalent with that of one individual, isolated, fracture in an elastic medium. See Figure 3-21 and related text in Fälth and Hökmark (2012) for a demonstration example.

As for the importance of the planarity of the target fractures in the 3DEC models, it has been demonstrated that a modest undulation of the fracture plane could suppress the shear displacements considerably. For a wavy fracture with an 11 degree deviation from the nominal fracture orientation, Lönnqvist and Hökmark (2015) found that the slip caused by a significant, destabilizing, increase of the shear load was only about 50% of the slip obtained on a corresponding planar fracture of the same size and orientation.

To get perspectives on the impact of fracture-fracture interactions (cf. last bullet above), results from a specifically designed specific example model are shown in Figure 2-3. The model is based on one of the Olkiluoto models mentioned above. In a specific version of the model, a DFN network was defined in a volume containing one of the target fractures that slipped most in response to the earthquake in the base case version of the model (Figure 2-3, left). Figure 2-3 (right) shows the impact of the DFN network: the secondary slip on the selected target fracture was reduced by about 20%. This result confirms that a fracture network will tend to reduce the largest displacements that would be obtained for corresponding isolated fractures.

Applying the simulation method to a site-specific Forsmark model and accounting for all of the conditions in the bullet list above, the largest secondary displacement found among the numerous differently positioned and oriented target fractures at 200 m distance on the footwall side of the ZFMA2 zone, (i.e., corresponding to where the deposition areas are located) was less than 30 mm (Fälth 2015). This result regards an earthquake occurring under end-glacial conditions, i.e., under conditions when the seismic activity in the Fennoscandian shield is expected to increase mainly because gently dipping deformation zones, such as ZFMA2, will be destabilized. For a corresponding thermally induced earthquake, or a present-day earthquake, the induced displacement would be even smaller (Fälth and Hökmark 2013).

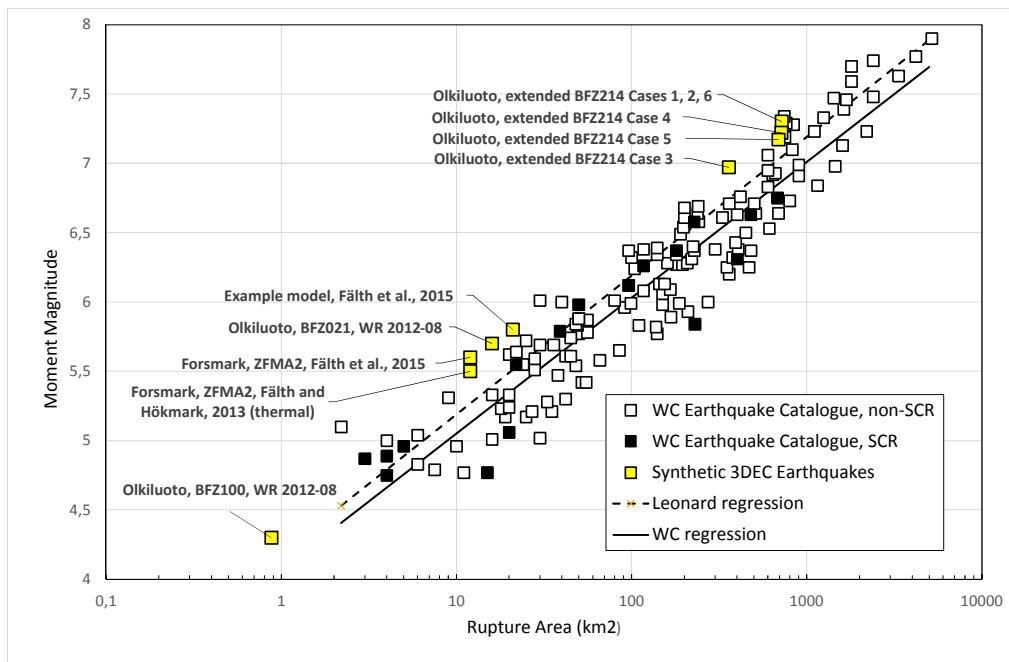


Figure 2-1. Synthetic 3DEC earthquakes plotted along with data from Wells and Coppersmith (1994). The BFZ214 models are based on hypothetically extended versions of the BFZ214 deformation zone with fault areas large enough to accommodate, at least theoretically, earthquakes of magnitudes around Mw 7. In general the synthetic earthquakes plot above the regressions with considerable margins.

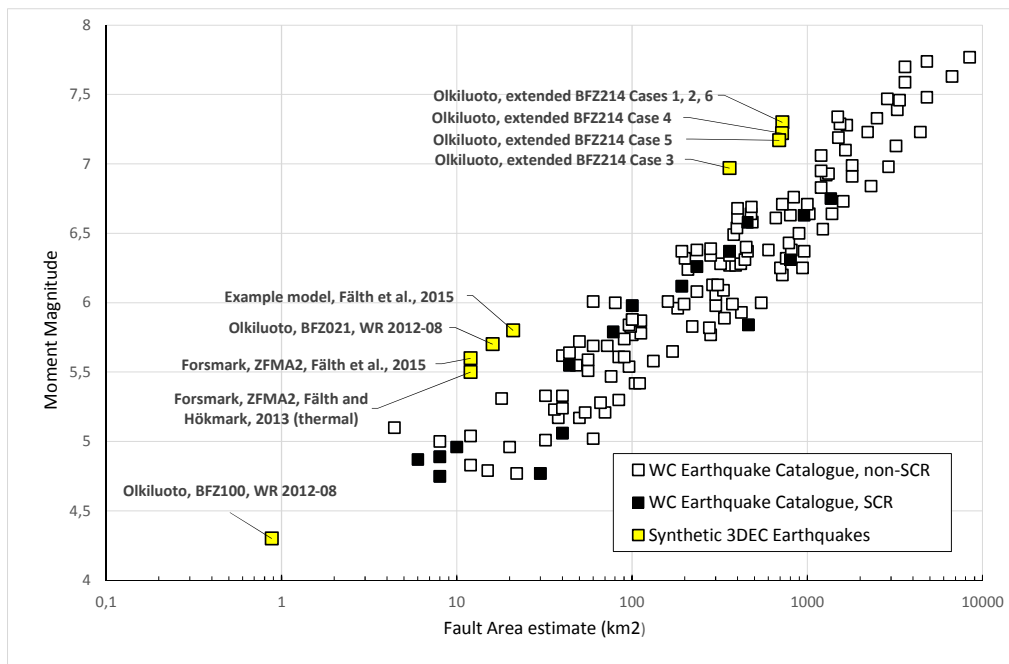


Figure 2-2. Same as Figure 2-1, but magnitudes given vs fault area instead of vs rupture area. For the synthetic earthquakes the fault area is the same as the rupture area. For the catalogue earthquakes, the fault areas have arbitrarily been set to be twice the rupture area.

3DEC DP 5.00
©2013 Itasca Consulting Group, Inc.

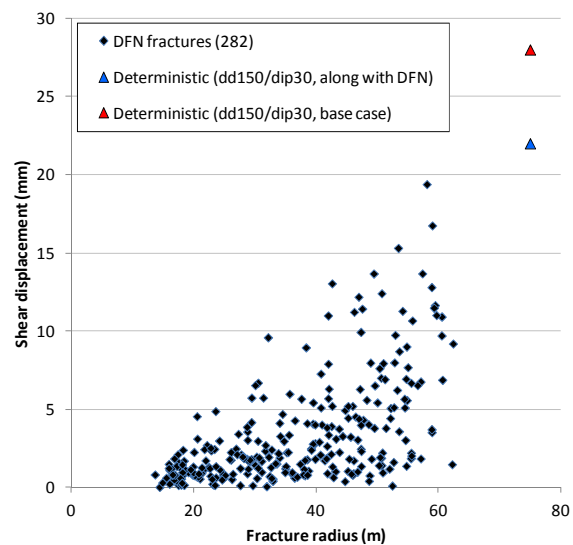
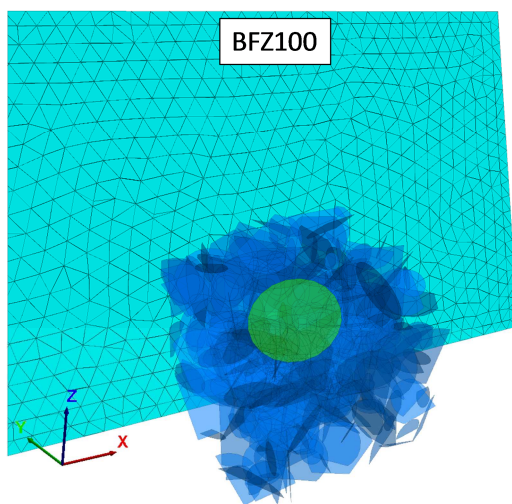


Figure 2-3. Left: Selected target fracture in surrounding DFN network. Right: secondary induced displacements on selected target fracture (triangles) and on DFN fractures (diamonds). The blue triangle shows the displacement with DFN network present, while the red triangle shows corresponding result for the isolated target fracture.

2.5 Ongoing and planned work

The results of the additional applications of the 3DEC modelling approach appear to confirm, with good margins, the relevance of the handling of the earthquake scenario in SR-Site. It remains to

ensure that the validity of the results is not unduly sensitive to variations in values of parameters that have not been systematically explored:

- Location of hypocentre (centre of fault in models analysed so far),
- Rupture velocity (70% of shear wave velocity in models analysed so far)

It also remains to check that the results are not unduly sensitive to different types of interactions between the primary fault and neighbouring deformation zones.

Results relevant to the issues above are presented in (Fälth et al. 2015a)

2.6 Perspectives on the degree of conservativeness

Most results obtained so far are based on conservative, or very conservative, assumptions: maximized magnitudes, perfectly planar target fractures, abrupt arrest of rupture at artificially sharp fault edges, etc. Making realistic, best estimate, assumptions regarding all these issues is likely to reduce the induced target fracture slip sufficiently that the seismic risk, i.e., the risk of damage to canisters caused by shear displacement along intersecting fractures, effectively vanishes. The results could then not necessarily count as robust upper bound slip estimates. Making slightly more realistic assumptions regarding a few of the issues might, however, give meaningful perspectives on the conservativeness and, possibly, pave the avenue for a more efficient use of the rock volume designated for the repository. In Figure 2-4, upper left, a number of the conservatively handled issues are listed. "X" denotes the largest resulting target fracture displacement (given, for instance, as slip per unit of fracture diameter). In the other sub-figures, the influence of changes made in the handling of some of the issues are shown. The reductions of the maximum target fracture slip shown here are approximate. Some are based on reported results (Fälth and Hökmark 2015; Lönnqvist and Hökmark 2015) or on results given in studies submitted for publication (Fälth et al. 2015a).

Figure 2-4, lower left, regards the moment magnitude: Earthquakes of magnitudes plotting on, or close to, the Leonard regression rather than above it (c.f. Figure 2-1) produce substantially smaller secondary displacements. For the Olkiluoto BFZ214 model described in Fälth and Hökmark (2015) the maximum displacement was reduced by about 50% when the rupture process was modified to give lower, but still relatively high magnitudes. For the Forsmark ZFMA2 model described in (Fälth et al. 2015a) similar results were obtained (see special section below for details).

Figure 2-4, upper right, regards the planarity of the target fractures. In all 3DEC dynamic simulations performed to assess the potential for large secondary fracture shear displacements, the target fractures have been modelled as perfectly planar. Lönnqvist and Hökmark (2015) showed, using static 3DEC models, that modest undulations would reduce the largest displacements by around 50% (See special section below for details).

Figure 2-4, lower right, concerns the effect of disregarding inelastic deformations in the rock mass surrounding the target fractures. The results of the test model described in Figure 2-3 and associated text corresponds to a reduction of maximum slip of around 20% if the slipping target fracture is located within a 3D fracture network rather than within an elastic continuum. However, this issue has not yet been systematically assessed and is subject to ongoing efforts.

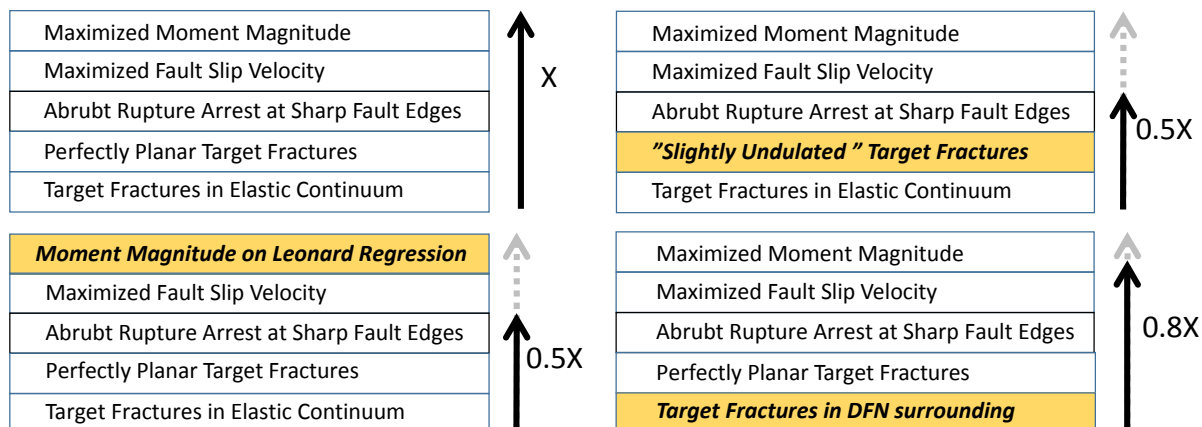


Figure 2-4. Simulation issues of importance to the response of target fractures modelled in the rock mass surrounding the earthquake fault. Here "X" denotes the maximum displacement obtained in case all the conditions listed in the upper left are met. Examples are shown of approximate slip reductions following realistic modifications of some of the issues.

2.6.1 Magnitude overestimate

Figure 2-5 shows the magnitudes (red triangles) of the modified versions of the ZFMA2 and BFZ214 models along with the maximized magnitudes shown in Figure 2-1 (yellow squares). Also the modified models appear to be on the conservative side. A more fair comparison between the synthetic earthquakes and the real database earthquakes would be if magnitudes were given vs fault area rather than vs rupture area as in Figure 2-2: this would push the database plot symbols to the right and indicate clearly that also the modified model versions (red triangles) are well on the conservative side.

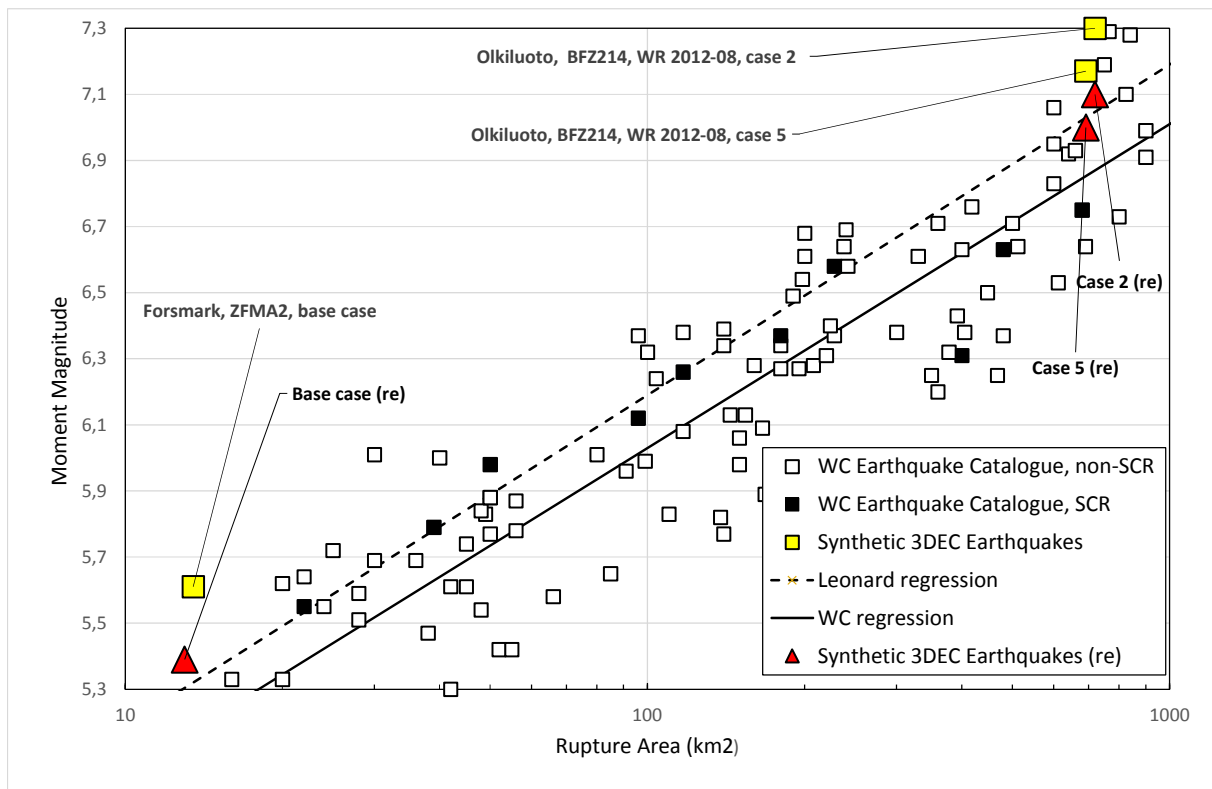


Figure 2-5. Close-up of plot shown in Figure 2-1, with synthetic earthquake results included only for cases for which also alternative versions with reduced magnitudes have been analysed (red triangles). The Olkiluoto models are described in (Fälth and Hökmark 2015) and the Forsmark models in (Fälth et al. 2015a)

In Figure 2-6, secondary target fracture displacements at different distances and at different positions along the strike of the BFZ214 deformation zone are shown for the two cases included in Figure 2-5: Case 2 and Case 5. Results are given for the maximized magnitude versions (yellow squares in Figure 2-5) and for the reduced magnitude versions (red triangles in Figure 2-5). The reduced magnitude earthquakes systematically produce target fracture displacements that are about 50% of those produced by the maximized magnitude earthquakes. Note that the largest slip appear to occur as a result of local stress concentrations formed around sharp edges of the stability strip in the Case 5 model. Also these displacements are reduced by about 50% when the magnitude is reduced to a less exaggerated value.

Figure 2-7 shows secondary slip at different distances from Forsmark deformation zone ZFMA2 for the maximized magnitude model (yellow square in Figure 2-5) and for the reduced magnitude version (red triangle in in Figure 2-5) (Fälth et al. 2015a). Again the largest secondary displacements are reduced by about 50% when the magnitude is reduced to a less exaggerated value.

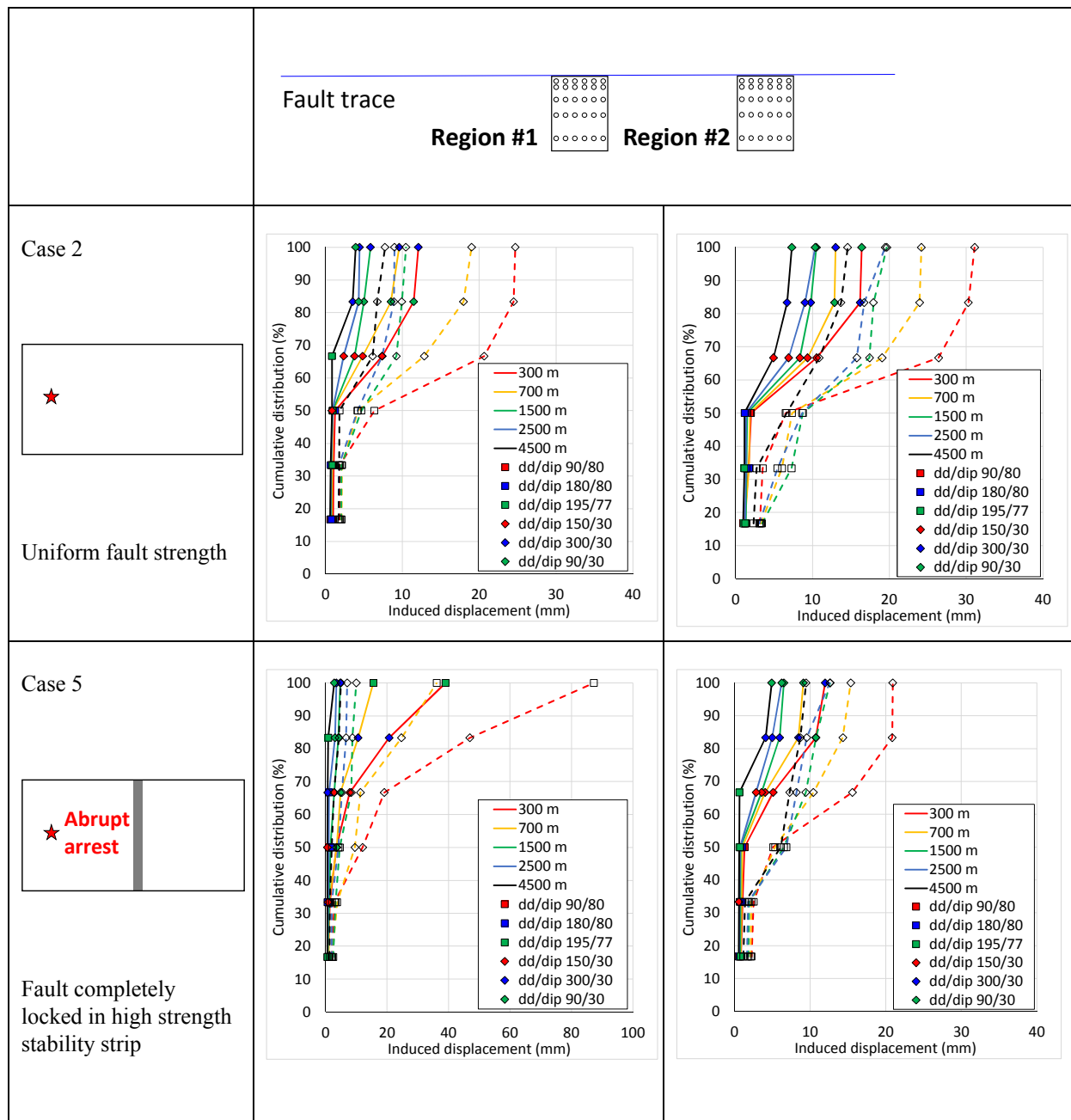


Figure 2-6. Seismic response of 300 m diameter target fractures, located at different distances from rupturing 720 km² version of Olkiluoto deformation zone BFZ214 (Fälth and Hökmark 2015). The target fractures are located in two separate regions as shown in the top row of the figure. The slip results are shown accordingly in two separate columns. Two cases are considered here, both with the rupture initiated at fault midheight a few km from the fault edge: Case 2 with uniform fault properties and Case 5 with a narrow and sharp high stability strip reaching from the ground surface down to the lower fault edge. The dotted lines show slip results obtained in the maximized magnitude models indicated by yellow squares in Figure 2-5. The full lines show corresponding results obtained in models with reduced magnitudes, i.e., those indicated by red triangles in Figure 2-5. Note the different horizontal axis scale for Case 5, region #1. Note also that (with exception of Case 5, region #1) the steeply dipping fractures (squares) do not slip by amounts larger than 10 mm at any distance.

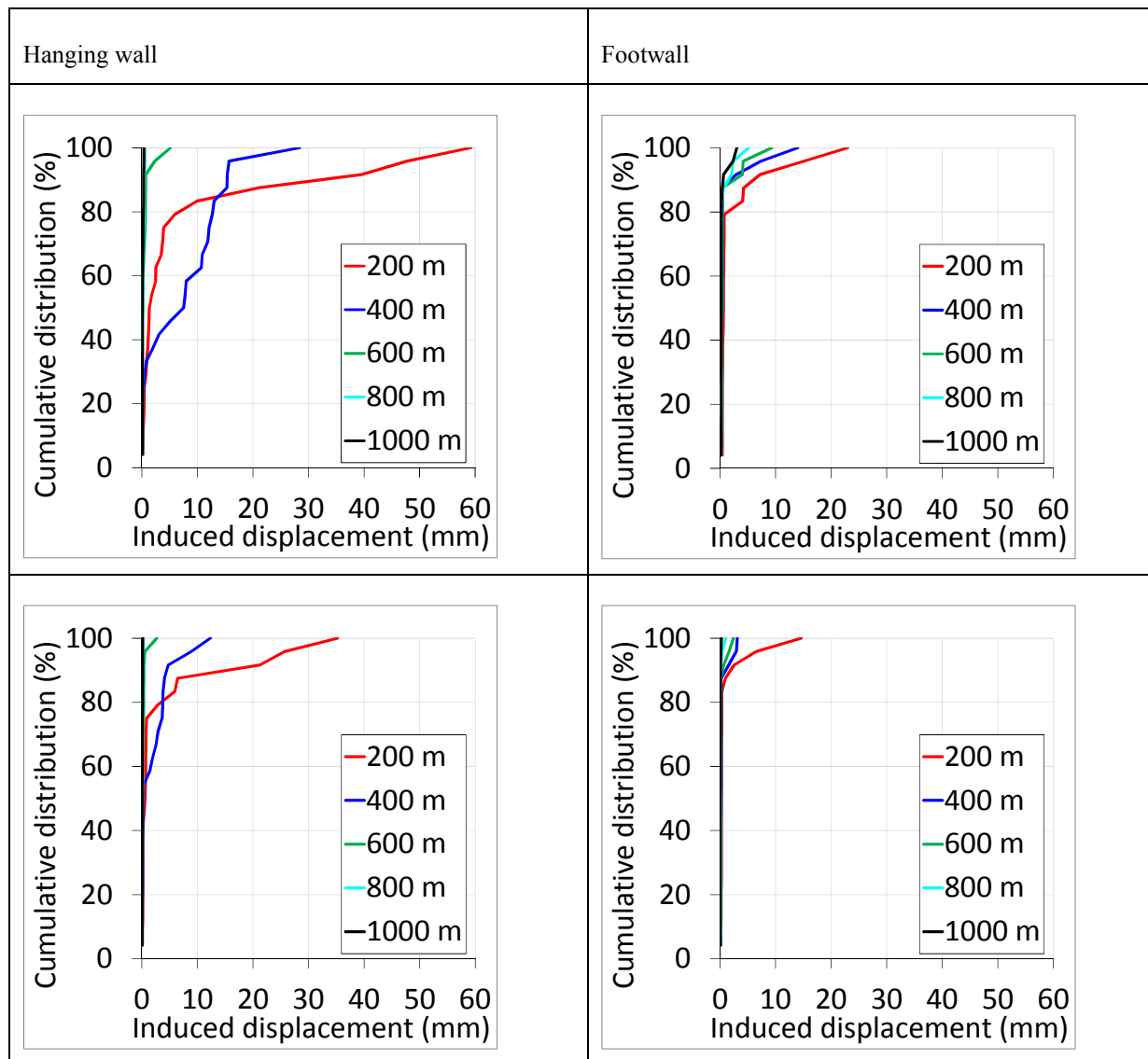


Figure 2-7. Seismic response of 300 m diameter target fractures at different distance from 13 km² rupturing ZFMA2 Forsmark deformation zone (Fälth et al. 2015a). The Forsmark deposition areas will all be located in the footwall side (right column). Upper: secondary slip resulting from magnitude 5.61 earthquake (yellow square in Figure 2-5). Lower: corresponding results for magnitude 5.39 earthquake (red triangle in Figure 2-5).

2.6.2 Planarity of target fractures

All 3DEC target fractures considered so far in dynamic models have been perfectly planar. Lönnqvist and Hökmark (2015) used static 3DEC models to explore the potential for modest geometrical disturbances of the fracture surface to reduce the slip following a load increase on a critically oriented fracture. Figure 2-8 shows result examples. A 200 m diameter fracture was undulated as shown in the top part of the figure and subjected to a significant load increase. As shown in the two diagrams, the effects of modest disturbances is significant. Even if the slip reductions obtained in these examples are very approximate and based on simplistic descriptions of the fracture surfaces (i.e., without consideration of stiffness variations, mechanical aperture variations etc.), it is evident that the default assumption of perfectly planar target fractures will contribute to give significant overestimates of the largest secondary displacements, such as those presented in, for instance, Figure 2-6 and Figure 2-7.

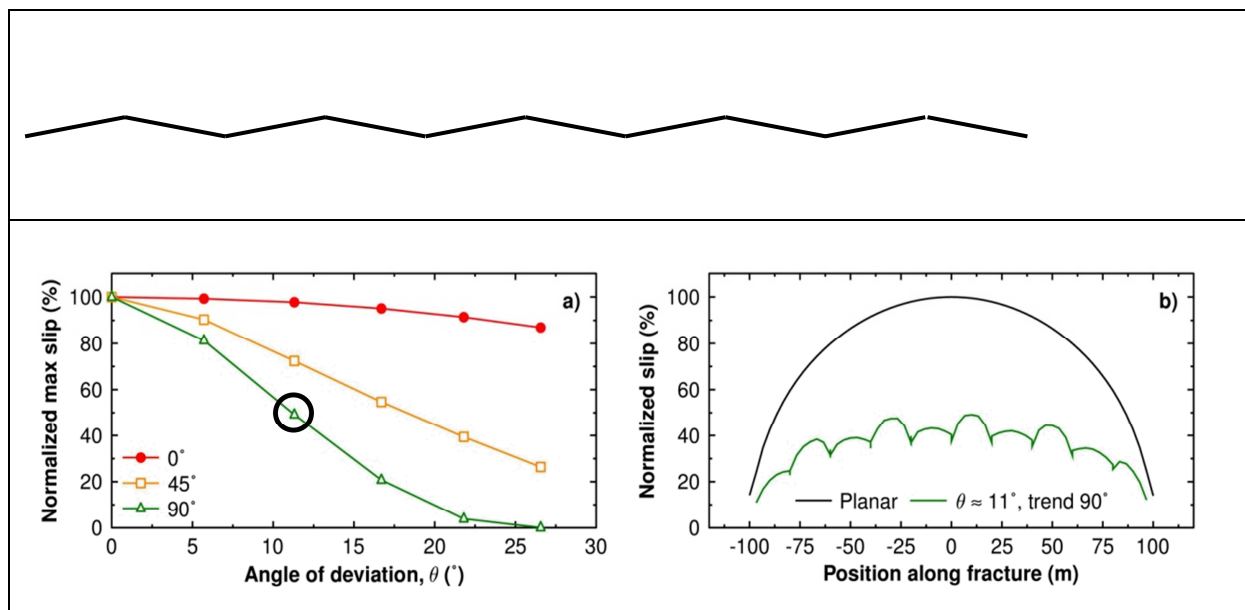


Figure 2-8. Top: 200 m diameter undulated fracture with 11 degree deviation from the average orientation of the fracture plane. Bottom left: Slip, normalized to corresponding planar fracture slip, for different deviation assumptions and for three assumptions of the orientation of the waves/ridges in relation to the shear direction. Bottom right: Normalized slip distribution along fracture diameter for case marked with circle in lower left (from Lönngqvist and Hökmark 2015).

2.6.3 Representation of fault edges

We have found that the largest secondary displacements systematically occur in response to local stress concentrations formed around artificially sharp fault edges. This is the case for the Forsmark models (Fälth and Hökmark 2013; Fälth et al. 2015a; Fälth et al. 2015b) as well as for the Olkiluoto models (Fälth and Hökmark 2011, 2012, 2015). The rupture and the associated loss of shear strength is allowed to propagate without restrictions until it is abruptly arrested at the edges. This is obviously a much too simplistic description of the conditions that limit the rupture propagation and determine the size and shape of the rupture area. In real earthquakes rupture propagation is more likely to die out successively when regions of the fault plane with high, but not infinite, strength are getting involved. Figure 2-9, left, shows an example of effects of sharp edges in an Olkiluoto BFZ214 model. Here the target fractures located close to a stability strip with sharp edges at the smallest distances (300 m and 700 m) from the fault slip by very significant amounts (c.f. Figure 2-6 above). If the edges are less sharp, i.e., the stability strip is not completely locked (Figure 2-9, right), the largest target fracture displacements are reduced by more than 75%.

The comparison made in Figure 2-9 between stress concentration effects around infinitely sharp fault edges (or, rather, rupture area edges), i.e., the type of edges modelled as standard up to the present day, and around more realistic strength variations, i.e., where the rupture is arrested successively, shows that the description of the way the rupture is arrested is an issue that would require a more systematic handling. Simulating the rupture propagation with a slightly less abrupt arrest at the edges of the slipping fault would result in significantly smaller maximum secondary displacements in all models with target fractures located close to fault edges.

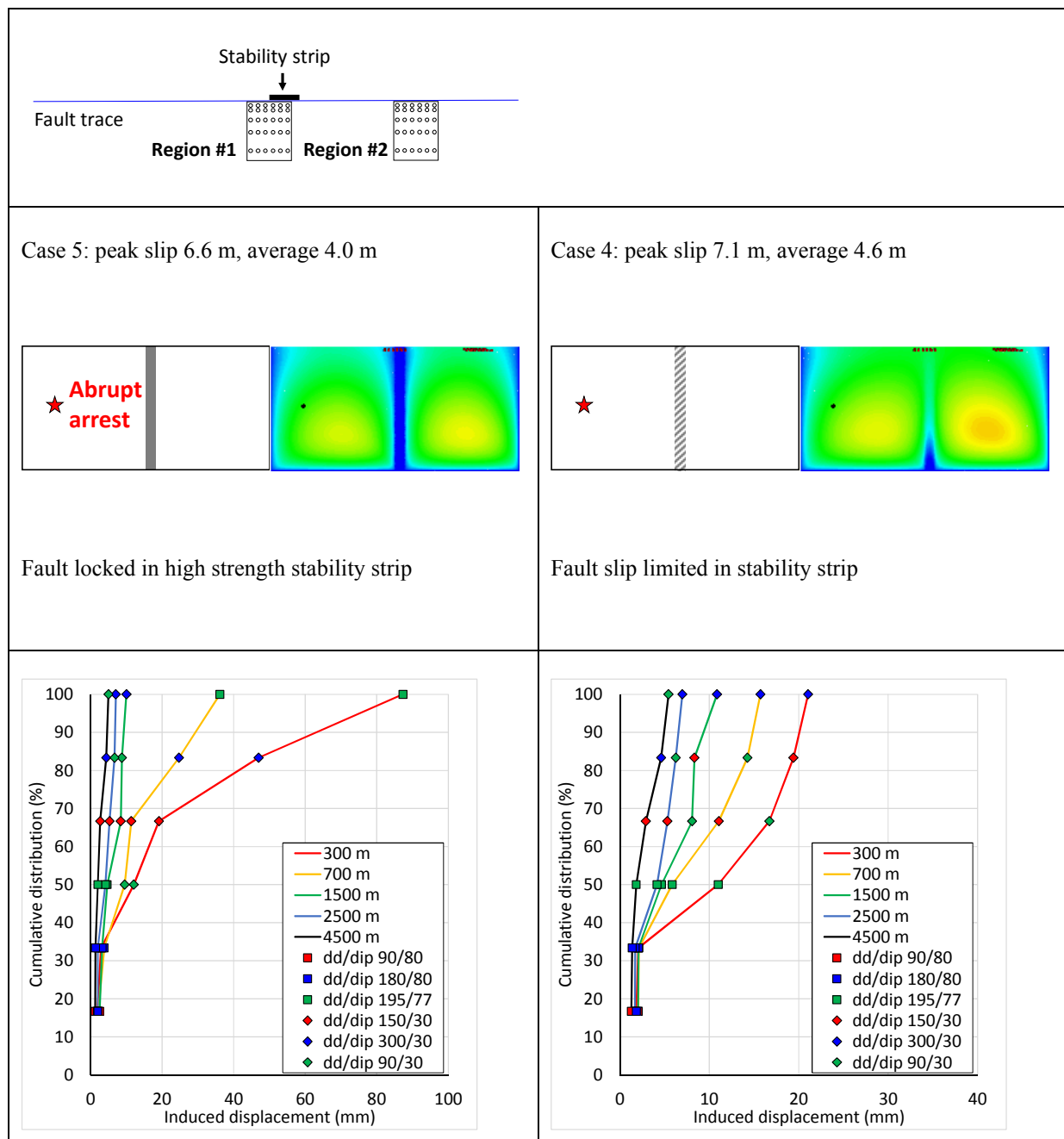


Figure 2-9. Upper: fault slip for cases with schematic fault inhomogeneities. Left: fault locked in stability strip. Right: finite strength in stability strip. Lower: corresponding secondary target fracture displacements (Fälth and Hökmark, 2015).

2.7 3DEC simulation method – summary

The 3DEC models analysed so far have deliberately been based on conservative, or very conservative, input assumptions. As demonstrated in the previous sections, making slightly more realistic assumptions regarding one or two issues would reduce the maximum secondary displacements quite significantly. Modifying the modelling approach towards a more realistic, but sufficiently

conservative, assessment of the coseismic response of the Forsmark rock mass must be carried out in a defensible step-by-step manner.

3 Comments on the modelling results in Yoon et al. (2014)

Below, we comment on the modelling approach and the modelling results in Yoon et al. (2014). We have concerns about the relevance of the approach and the interpretation and handling of the results and, consequently, also about the recommendations to SKB made in the report:

- The use of two-dimensional models to problems for which the three-dimensional aspects are critically important.
- The handling and interpretation of numerical errors as “outliers”.
- The lack of discussion of unrealistic modelling results.

3.1 Problems associated with the of 2D approach

3.1.1 Slip of individual fractures

To be useful, a numerical model method must capture the most important aspects of the system under study while ignoring less important ones. For the safety assessment and for layout decisions, the issue is to establish safe upper bound estimates of the largest fracture shear displacements, i.e., shear displacements caused by stress changes significant enough to push the entire fracture area well over the stability threshold. Such displacements will critically depend on the orientation relative to the stresses and on the fracture size.

For a circular fracture with radius a , the displacement $u(r)$ at distance r from the fracture centre is given by

$$u(r) = \frac{8}{\pi(2-\nu)} \frac{(1-\nu)}{G} \Delta\tau \sqrt{a^2 - r^2},$$

where G is the shear modulus of the surrounding rock, ν Poisson’s ratio and $\Delta\tau$ the stress drop associated with the slip (Segedin 1951). The corresponding expression for a two-dimensional fracture, i.e., a fracture that extends infinitely in the out-of-plane direction, reads (Starr 1928):

$$u(r) = \frac{2(1-\nu)}{G} \Delta\tau \sqrt{a^2 - r^2}.$$

Here $2a$ is the length of the fracture in the modelling plane and r the distance to the fracture centre.

For values of Poisson’s ratio typical of crystalline rock (≈ 0.25), the 2D expression appears to overestimate the displacement by about 40% for fractures perfectly perpendicular to the 2D section in which they are modelled. If the modelling plane coincides with the $\sigma_1 - \sigma_3$ principal stress plane, the slip overestimate will be even larger for the majority of the fractures. The orientation of the fracture relative to modelling plane will determine exactly how much larger this overestimation will be.

3.1.2 Fracture interaction and plastic deformations

Yoon et al. (2014) correctly argue that the modelling approach used in SKB's assessment of the seismic risk does not allow for elasto-plastic rock behaviour, potentially leading to fracture growth and fracture coalescence, to be considered. It should be noted, however, that the practical consequences of this are negligible:

The SKB assessment of the seismic risk is not based on predictions attempted to capture the details of a realistic response of a real fractured rock mass with interacting, non-planar, fractures. Instead, the assessment of the seismic risk is based on 1) robust upper bound estimates of seismically induced shear displacements along pessimistically idealized, perfectly planar, rock fractures that potentially could intersect canister positions and 2) protocols, devised to identify potentially critical (i.e., large) fractures during construction and to reject canister positions intersected by such fractures.

Coalescence of relevantly sized fractures is not likely to produce fractures of shapes (footprint and degree of planarity) that would allow slip of magnitudes similar to those of the slip of corresponding circular, perfectly planar, 3DEC fractures of the same fracture area. In addition, strain energy will have to be expended on rock failure processes in order for coalescence to occur, which will reduce the strain energy available to power slip on the resulting fracture. Additionally, two fractures, located and oriented such that it would be a theoretical possibility for them to coalesce and form a large, continuous and reasonably planar fracture, are most likely to be identified as a single structure during detailed investigations, i.e., potentially critical canister positions would be rejected anyhow.

Regardless of whether or not fracture growth and fracture coalescence would be processes of practical consequence for layout decisions and risk assessment, a 2D model cannot capture the scope and extent of these processes in a fractured rock mass. Even if the two neighbouring 3D fractures in Figure 3-1 (left) would be optimally oriented for coalescence, which regardless of their actual orientations is always the case in a 2D representation of a fracture network (Figure 3-1 centre and right), the geometry of the 2D rock bridge (Figure 3-1, right) does not have much in common with the real 3D rock bridge. Moreover, because of the exaggerated slip along the 2D fractures (overestimate typically about 40%; see above) the stress concentrations around the fracture tips and the conditions for rock bridge failure and coalescence are extremely overestimated.

We claim, based on the above, that a 2D modelling approach is inadequate when it comes to capturing the scope and extent of coalescence in a rock mass with a three-dimensional fracture network.

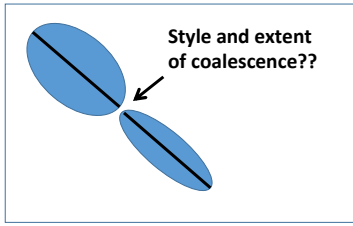
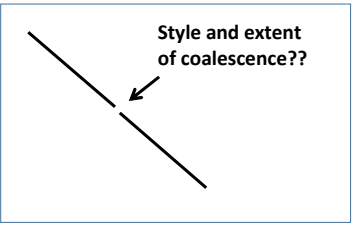
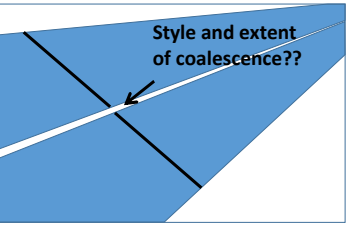
		
Rock bridge between two neighbouring 3D fractures	2D representation of rock bridge	3D equivalent of 2D representation of rock bridge

Figure 3-1. Left: Example of neighbouring fracture geometry in 3D space. Middle: 2D section. Right: Physical 3D equivalent of 2D representation.

3.1.3 Thermal loads

The thermal load generated by the decaying nuclear waste varies in all directions and cannot be correctly captured on a scale relevant to the problem of thermally induced shear displacements along deformation zones and large fractures, unless the 3D aspects are adequately accounted for.

The 2D models analysed in Yoon et al. (2014) do all regard horizontal sections, meaning that effects of stress variations (both vertical and horizontal) with depth are ignored. During the early phases of the temperate period these variations are considerable and contribute to determine the stability evolution of deformation zones located within or in the vicinity of the heated regions. After some 50 years the horizontal stress additions are significant only within a limited depth interval around the repository horizon, cf. Figure 6-16 in SKB's assessment of the thermomechanical evolution of the Forsmark host rock (Hökmark et al. 2010). This fundamental aspect of the thermal load is not captured by the 2D model used in Yoon et al. (2014).

Because of differences in vertical expansion between heated and non-heated regions, the vertical stress will increase in deposition areas and decrease between and just outside deposition areas. This mechanism will influence the stability evolution of differently located fractures in a way that cannot be captured in 2D models of horizontal sections. As shown in SKB's 3D assessment of the thermomechanical evolution of the Forsmark host rock, fractures located within the deposition areas will be significantly more stable than fractures located between or just outside the deposition areas, cf. Figure 3-2. As a consequence, the most unstable fractures within the deposition areas will slip significantly less in response to the thermal loading than similarly oriented and sized fractures located between or just outside the deposition areas, cf. figures 6-27 and 6-28 in SKB's 3D assessment (Hökmark et al. 2010). This is not captured in the 2D study of Yoon et al. (2014). On the contrary the authors claim that *"From the modelling of heat induced repository responses, it is observed that the repository rock mass expands due to the heat and induces shear displacement of the target fractures and the nearby deformation zones. Shear displacements are up to 12 mm for those fractures located within the footprint of the heated panels, and relatively smaller at the outskirts of the heated panels..."*.

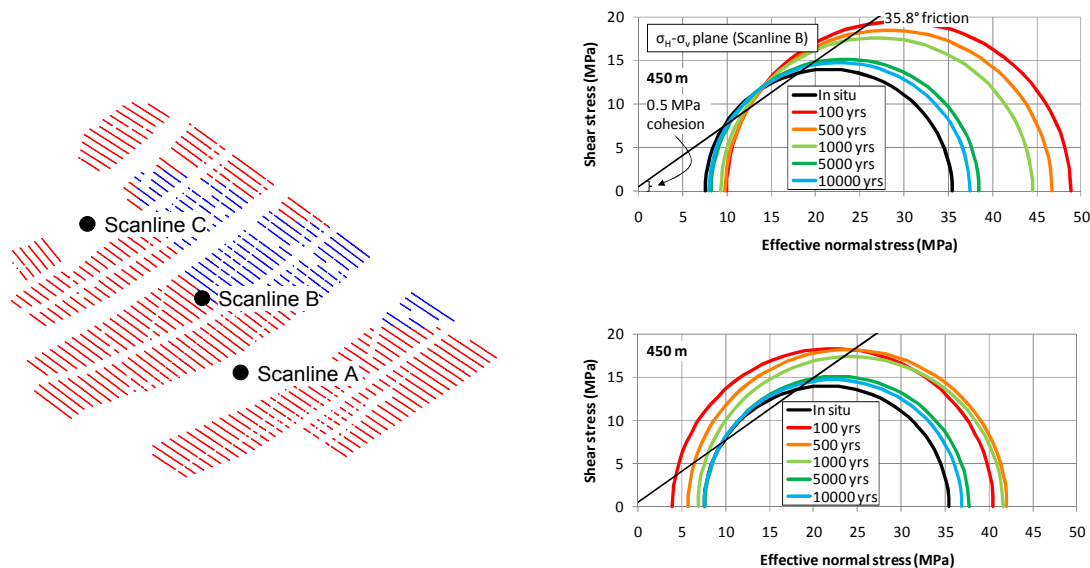


Figure 3-2. Left: Repository layout. The blue and red canister symbols correspond to the two different canister spacing regions specified in the layout. Right: Mohr circle representation of stress evolution within deposition areas (upper; intersection with scanline B) and between deposition areas (lower; intersection with scanline A). The increase in vertical stress within the deposition areas limit the thermally induced destabilization of gently dipping fractures, while the vertical stress reduction between deposition areas contributes to destabilize these fractures. As a consequence, fractures within the deposition areas slip less than corresponding fractures in the outskirts, i.e., not more, as claimed in Yoon et al. (2014). Figures from Hökmark et al. (2010).

The horizontal 2D models do not capture the potentially important stability loss of gently dipping fractures and deformation zones during the heated period (cf. Figure 3-2). As opposed to the vertical zones included in the assessment by Yoon et al. (2014), these structures (for instance the ZFMA2 deformation zone) could be close to failure already under the existing in situ stress conditions, cf. red Mohr circle in Figure 3-3 (stresses at repository depth). As illustrated by the blue Mohr circle in the same figure, vertical deformation zones are significantly more stable. The effect of heating (increase of both horizontal principal stresses) is to stabilize the vertical deformation zones further, i.e., push the blue Mohr circle further to the right. Yet, in their modelling of thermally induced seismic events, the authors assume four earthquakes with moment magnitudes ranging approximately between 1.6 and 2.3 to occur simultaneously after some time of heating, each in one of the heated deposition areas (see Figure 3-4 for an example). These modest seismic events result, together with the thermal impact, in rock mass failure and strike-slip shear displacements along target fractures. The inelastic irreversible response of the repository rock mass to the four microquakes and the heating is sufficiently extensive that the major horizontal stress decreases by about 1 MPa on average (cf. Tables 10 and 11 in Yoon et al. (2014). The minor horizontal stress increases by less than one half MPa on average. These stress reductions occur within the repository footprint (area number 1, 3 and 4 in Tables 10 and 11; see Figure 22) as well as outside the footprint (area number 2 and 5).

These modest (less than one MPa) changes of the *in situ* stresses after 25 years of heating should be compared with the thermal stress estimates presented in SKB's 3D analysis of the thermomechanical evolution of the Forsmark host rock: within the heated areas the two horizontal stresses increase by 13 – 15 MPa after 50 years at the large scale, cf. Figure 6-16 in (Hökmark et al., 2010). After 5 years the increase is about 5 MPa, see also results given for the local scale in Figure 43 in Yoon et al.

(2014). The results presented in Tables 10 and 11 of Yoon et al. (2014) mean that target fracture slip and rock mass failure has eliminated the thermal stresses after 25 years (Figure 3-5). We argue that this result is unrealistic:

Before heating, the target fractures in the horizontal 2D section in Yoon et al. (2014) are all subjected to the stresses represented by the blue Mohr circle in Figure 3-3, meaning stability margins of at least 10 MPa. These margins increase when the horizontal thermal stress additions push the blue Mohr circle further to the right. There is no mention in Yoon et al. (2014) on whether or not any pore pressure is included. If not, the Mohr circle should be moved another 4-5 MPa to the right. We do not agree that a systematic and extensive release of strain energy, such as the one suggested by the results presented in Yoon et al. (2014) (around 10 MP relaxation in the heated regions), can be triggered by microquakes in a rock mass with all fractures having stability margins in the order of 10 MPa.

There is no description of the temporal stress evolution at repository depth during heating, so it is not possible to establish exactly in what way and to what extent the 2D approach specifically has contributed to the unrealistic results.

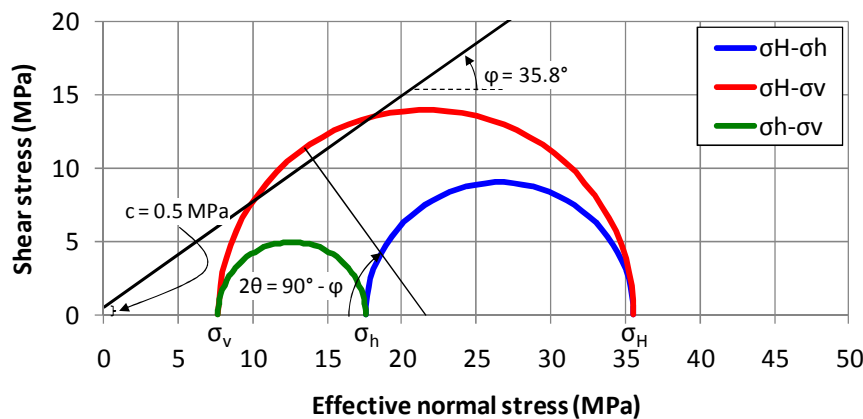


Figure 3-3. Mohr circle representation of most likely in-situ stress state (Martin 2007) at repository depth assuming hydrostatic pore pressure. The stability of vertical fractures and deformation zones (i.e., those explicitly modelled in Yoon et al. (2014) is determined by the blue circle (from Hökmark et al. 2010), indicating considerable stability margins.

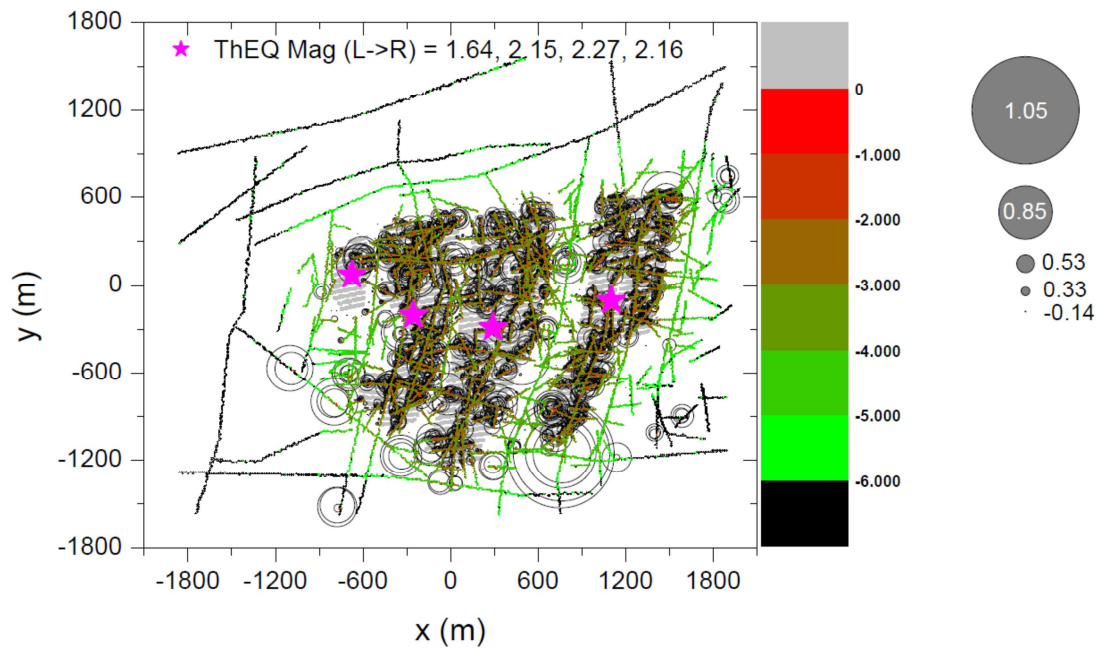


Figure 3-4. Microquakes (stars) and shear displacements 25 years after deposition. Figure A3-1 in Yoon et al. (2014).

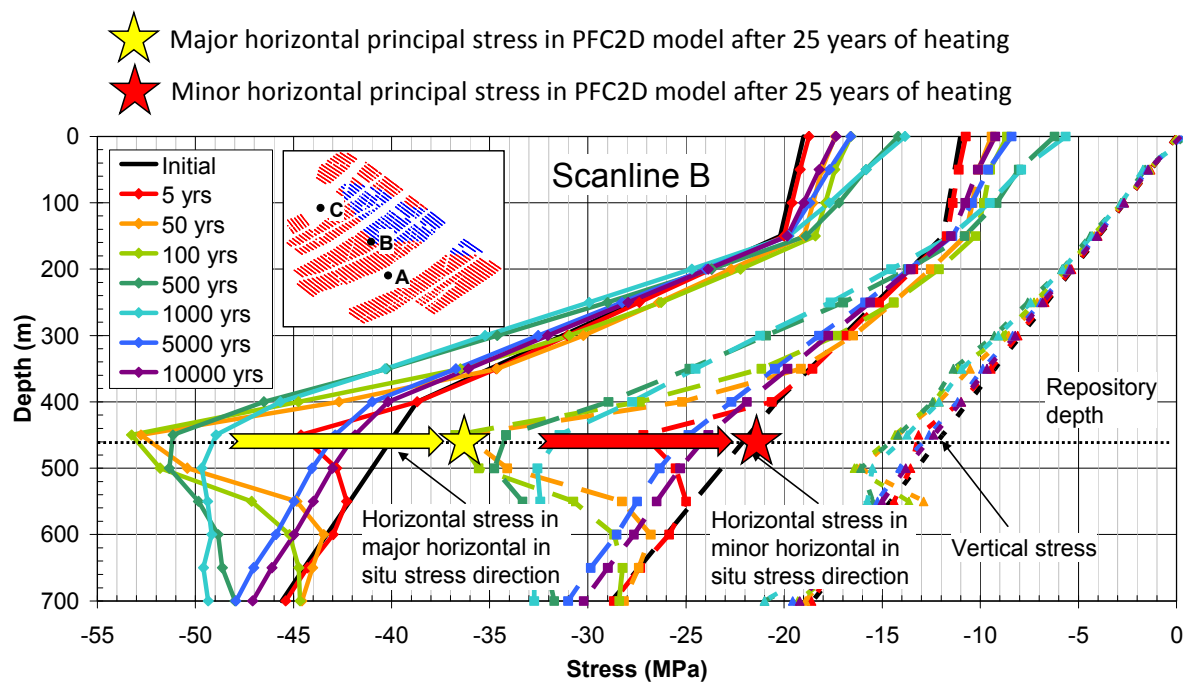


Figure 3-5. The figure shows the temporal evolution of the three principal stresses along a vertical scan line through the repository footprint (Scanline "B") as presented in SKBs assessment of the thermomechanical evolution of the Forsmark host rock (Hökmärk et al. 2010). The yellow and red stars indicate the major and minor stresses after 25 years of heating as calculated in Yoon et al. (2014, Table 10). The arrows indicate, approximately, the difference between the 3D stresses (3DEC) and the 2D stresses (PFC2D) after 25 years.

Finally, without going into the details of the temperature calculations, it should be noted that there are differences (cf. Figure 3-6) between the temperatures obtained after 50 years in Yoon et al. (2014) PFC2D model and in the SKB 3DEC model described in Hökmärk et al. (2010):

- In the PFC2D model, for instance, the rock temperature between deposition areas C and D has increased by 4 - 5 degrees 50 years after deposition, whereas there is practically no temperature increase in that region in the 3DEC model (cf. Figure 3-6). Similar differences can be observed, albeit not as clearly, for the more narrow non-heated regions between deposition areas A and B and areas B and C, respectively.
- In the PFC2D model there is no visible influence of the differences in thermal power density caused by differences in canister spacing (6.0 m between canisters in rock domain 29 and 6.8 m in rock domain 45 according to Layout D2 as shown in, for instance, Figure 5-10 in Hökmark et al. (2010), see Figure 3-7 below).
- In the PFC2D model, there seems to be little influence of canister positions being rejected along traces of intersecting deformation zones. In the 3DEC model intersecting deformation zones contribute to reduce the temperatures locally.

3DEC is based on an extensively tested implementation of analytical textbook solutions of the equation of heat conduction in 3D space. (The 3DEC results are not based on any “FEM-method” as stated in Yoon et al. (2014, p. 59)). The validity of the 3DEC results can easily be verified; see for instance Fälth and Hökmark (2006a) for a comparison between 3DEC temperatures and corresponding temperatures obtained using analytical solution devised by Claesson and Probert (1996). See also Lönnqvist and Hökmark (2013) for a comparison between temperatures measured in the Prototype Repository rock mass and corresponding temperatures calculated using 3DEC. There is no clear description of how out-of-plane heat flux (and variations in out-of-plane heat flux) is handled in Yoon et al. (2014), and therefore it is not possible to tell to what extent the 2D approach specifically has contributed to distort the results of the temperature calculation (faster horizontal propagation of the temperature front than in the 3D case, higher average footprint temperature than in the 3D case).

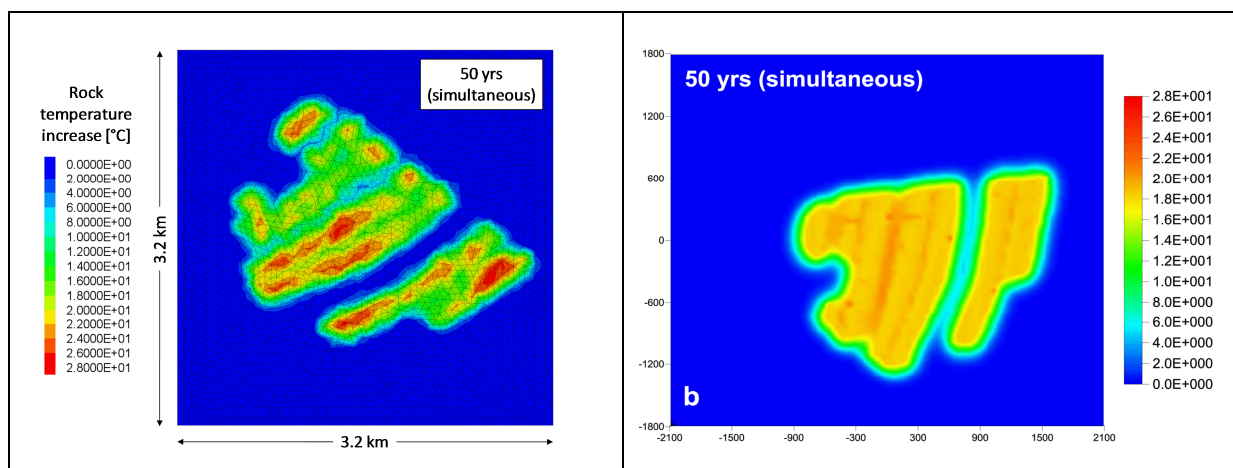


Figure 3-6. Temperatures at repository depth 50 years after simultaneous deposition of all canisters. Left: 3DEC solution (Hökmark et al. 2010). Right: PFC2D solution (Yoon et al. 2014).

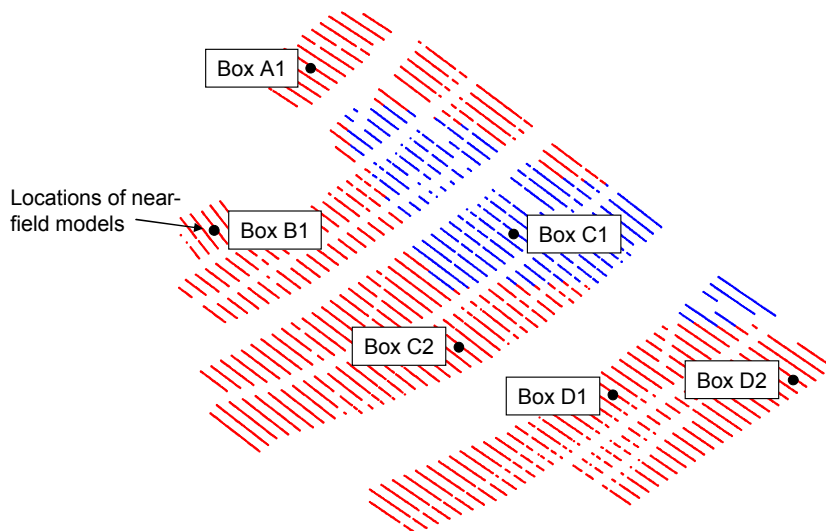


Figure 3-7. Layout D2 as implemented by Hökmark et al. (2010). Blue position markers mean 6.8 m canister spacing. Red markers mean 6.0 m spacing. Note also rejected canister position along traces of intersecting deformation zones.

3.1.4 Seismic loads

The seismic load generated by a nearby rupturing and slipping fault depends on the orientation of the fault plane in relation to the stress field, on how the stresses and the strength vary over the fault area, on the location of the hypocentre etc. None of these issues can be adequately addressed in a 2D model.

3.2 Impact and handling of “outliers”

Displacements above the 95th percentile and below the 5th percentile are arbitrarily and schematically regarded as “outliers” in Yoon et al. (2014). This means that results that potentially could belong to the most important ones, i.e., the largest fracture displacements, are automatically disregarded without ensuring whether or not those displacement are actually results of “local magnification effects and numerical singularities” as claimed by Yoon et al. (2014, p. 102).

Moreover, the application of the outlier criteria appears inconsistent and ill founded. Looking at Figure 3-8 (upper), and taking the results presented there at face value, it appears that a 70 mm shear displacement occurring on a 199 m fracture would be a trusted result, whereas a 50 mm shear displacement occurring on a 201 m fracture would count as a result of “local magnification effects and numerical singularities”. Target fracture displacements in the range 25 mm – 75 mm count as reliable or as outliers depending on the arbitrary subdivision in size classes.

Looking again at Figure 3-8 (upper) and taking Size Class 2 as an example, the mean displacement is found to be around 1.8 cm. Given that there are about 100 results in that size class, the total shear displacement (in that class) is around 1.80 m. About 0.7 m (around 40%) of that total shear

displacement appear to be due to outliers, i.e., claimed to be related to, or caused by, “local magnification effects and numerical singularities”.

On the level of the smooth joint displacement, similar relations between numerically disturbed displacement results (“outliers”) and total displacement seem to apply. Looking at, for instance, Figure A3-81 in Yoon et al. (2014, p. 176) (see Figure 3-9), it appears that the mean smooth joint displacements are sometimes just below, and sometimes just above, the 95% percentile, meaning that around 50% of the total slip is related to outlier displacements. The Class 11 mean displacement, for example, is around 7 mm, giving, in that class, a total smooth joint slip of around 4.2 m (given that about 600 results are shown for that distance class), to which outlier displacement appear to have contributed by more than 2 meters. Similar relations seem to hold for the other distance classes.

It is beyond the scope of this Memo to attempt to estimate to what extent, and exactly in what way, the large outlier contributions to the total displacement (50% of the total smooth joint slip and 40% of the target fracture slip potentially being related to numerical errors) has distorted the overall response of the 2D particle network and the fracture network in the different PFC models. Yoon et al. (2014) do not comment on this. Stress redistribution effects, stress release effects, intensity of fracture-fracture interactions and the extent of plastic deformation are, however, all likely to have been considerably exaggerated.

Looking again at Figure A3-81 in Yoon et al. (2014) (Figure 3-9), it appears that smooth joint displacements in the range 2 mm – 9 mm sometimes count as outliers, sometimes as reliable results, depending solely on the distance from the hypocentre to location of the slip event (or rather on the arbitrarily defined set of distance classes). This adds to the general uncertainty of the actual impact of the numerical errors.

3.3 Unrealistic results

3.3.1 Relation between fracture size and fracture shear displacement.

One of the objectives of the study presented in Yoon et al. (2014) is to explore relations between fracture size and fracture shear displacement (cf. report title). In the report no explicit statements are made regarding the outcome of this issue. The results presented in the report indicate, however, that the largest displacements in horizontal sections systematically occur on fractures with lengths ranging between 150 and 200 m (see Figure 3-8 below for examples). Larger fractures, subjected to the same seismic event, typically have maximum slips that are significantly smaller. This strange and counterintuitive finding does not agree with any theory or with results presented in the literature, and would consequently warrant a comment and a credible explanation.

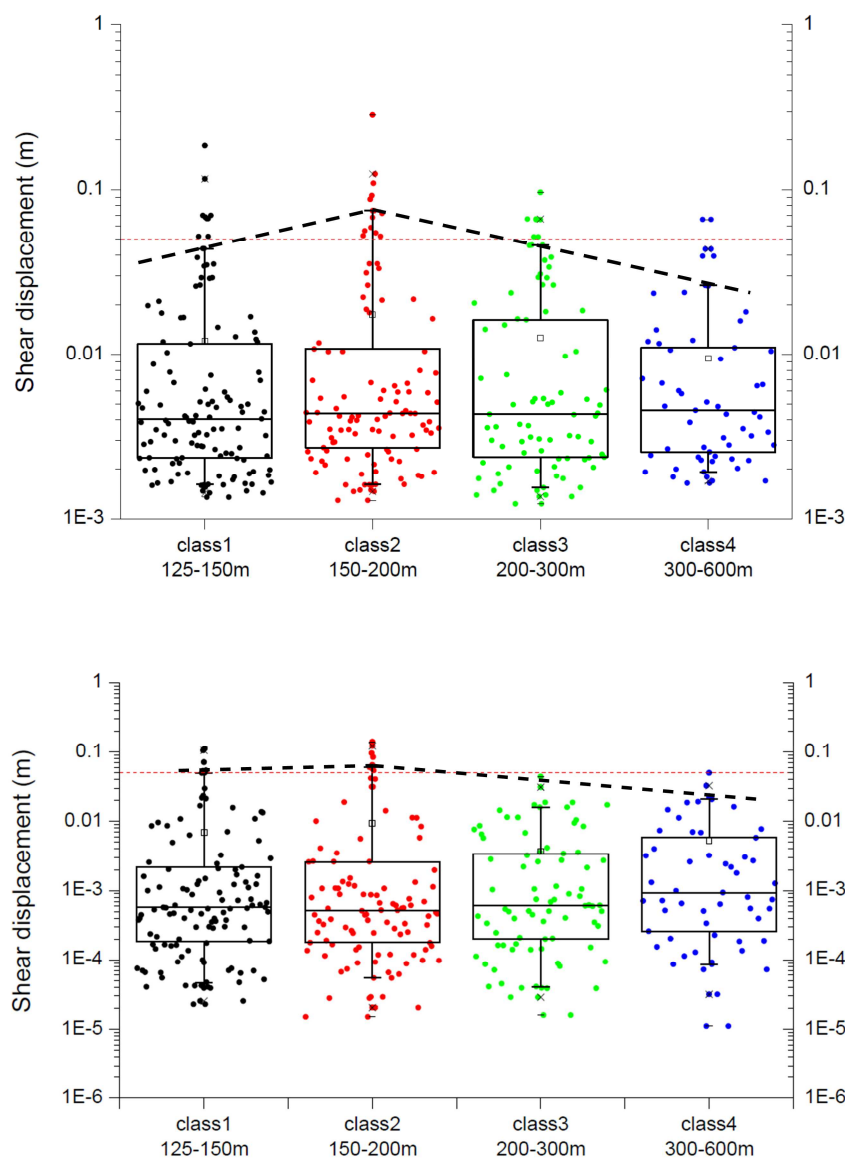


Figure 3-8. Upper. Response to forebulge earthquake on deformation zone ZFMWNW0001 (Singölinjen). Based on Figure A3-59 in Yoon et al. (2014). Lower: response to seismic event on ZFMWNW2225. Based on Figure A3-59 in Yoon et al. (2014). The largest trusted displacements systematically occur on fractures belonging to size class 2. Results above the dashed lines count as “outliers” resulting from “local magnification effects and numerical singularities”.

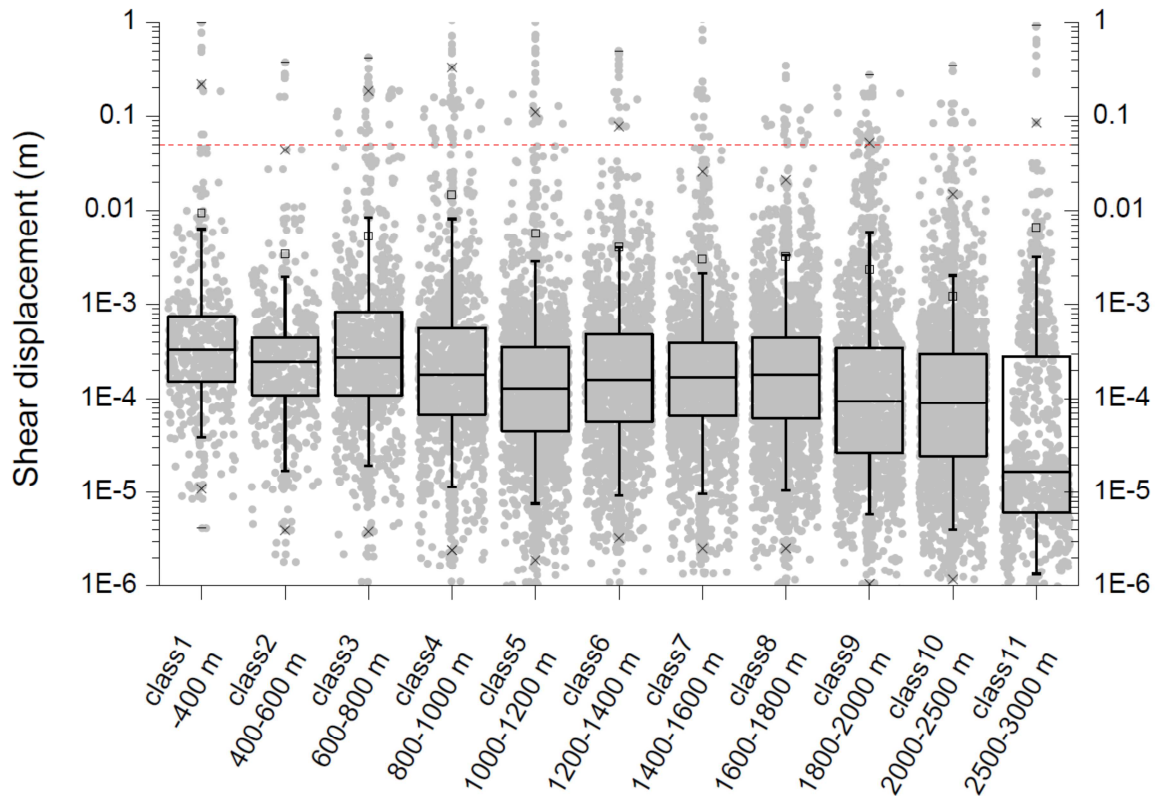


Figure 3-9. Smooth joint displacements in eleven classes of distance from hypocentre of earthquake on ZFMNW1200. Figure A3-81 in Yoon et al. (2014).

3.3.2 Fault size and fault slip

Figure 3-10 shows the primary fault slip assuming the Singö fault zone to rupture under forebulge stress conditions (Figure A3-63 in Yoon et al. (2014)). The figure also shows the slip induced on other deformation zones (squares) and on target fractures (circles). The PFC model fault trace length is less than 2.5 km (while it is assumed to be 15 km in the magnitude calculation). The mean fault slip value is 49 m. In a corresponding simulation in which the Singö fault zone ruptured under present day stress conditions, the mean fault slip amounted to 36 m. In Figure 3-11 these modelling results are plotted along with data compiled by Wells and Coppersmith (1994). The modelled mean fault displacements are about three times larger than the largest maximum fault displacement found in the Wells-Coppersmith database, i.e., that of the 1931 Kehetuohai, China, magnitude 7.9 earthquake with a surface rupture length of 180 km. The Singö fault mean slip, as calculated in Yoon et al. (2014), is about 5 times larger than the mean slip of the Kehetuohai earthquake.

The authors do not attempt to justify or explain how the extremely large primary slip mean values could be consistent with the size of the primary fault. The Wells-Coppersmith database includes shallow-focus (hypocentral depth less than 40 km) continental interplate or intraplate earthquakes of magnitudes greater than approximately 4.5. Earthquakes associated with subduction zones are not included. However, to match the fault slip obtained in the Yoon et al. (2014) modelling of an earthquake on the Singö fault zone, we need to compare with the largest interplate subduction zone

earthquakes ever instrumentally recorded, such as the 2011 Tohoku Magnitude 9.0 earthquake. Modelling of the rupture of this earthquake indicates that the fault slipped over an area approximately 400 km long (along-strike) by 200 km wide (in the down-dip direction), with an average slip of 18 m and a maximum slip of about 50 m (Lee et al. 2011). Numerous studies arrive at similar results, cf. for instance Yagi and Fukahata (2011).

The rupture length of the Singö fault earthquakes as pictured in, for instance, Figure A3-63 in Yoon et al. (2014) is 1% of the rupture length of the Tohoku earthquake. Yet, the mean Singö fault slip, as modelled by Yoon et al. (2014), is larger than the average slip of the Tohoku magnitude 9.0 subduction zone earthquake. This is beyond any reason and raises doubts about the modelling approach and the general credibility of the study.

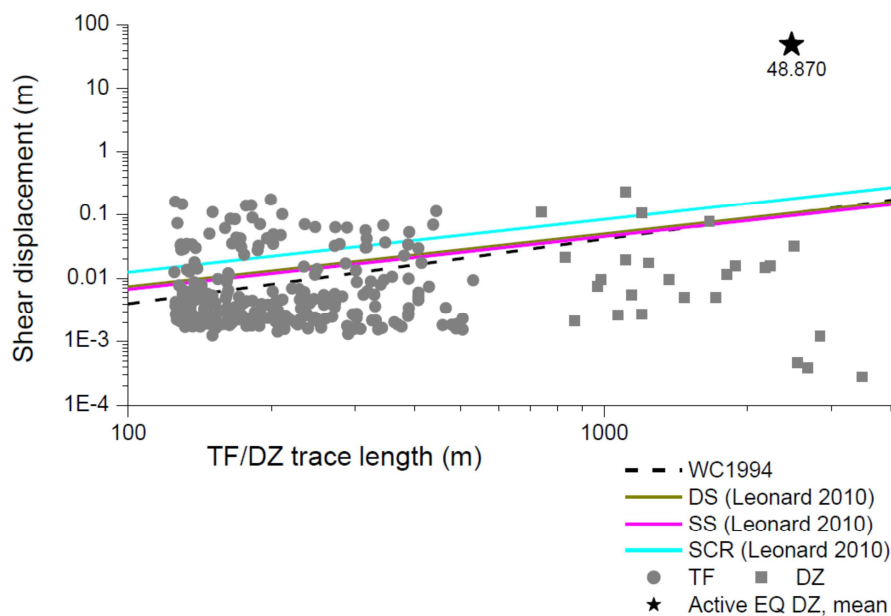


Figure 3-10. Response to forebulge earthquake on deformation zone ZFMWNW0001 (Singölinjen). Figure A3-58 in Yoon et al. (2014).

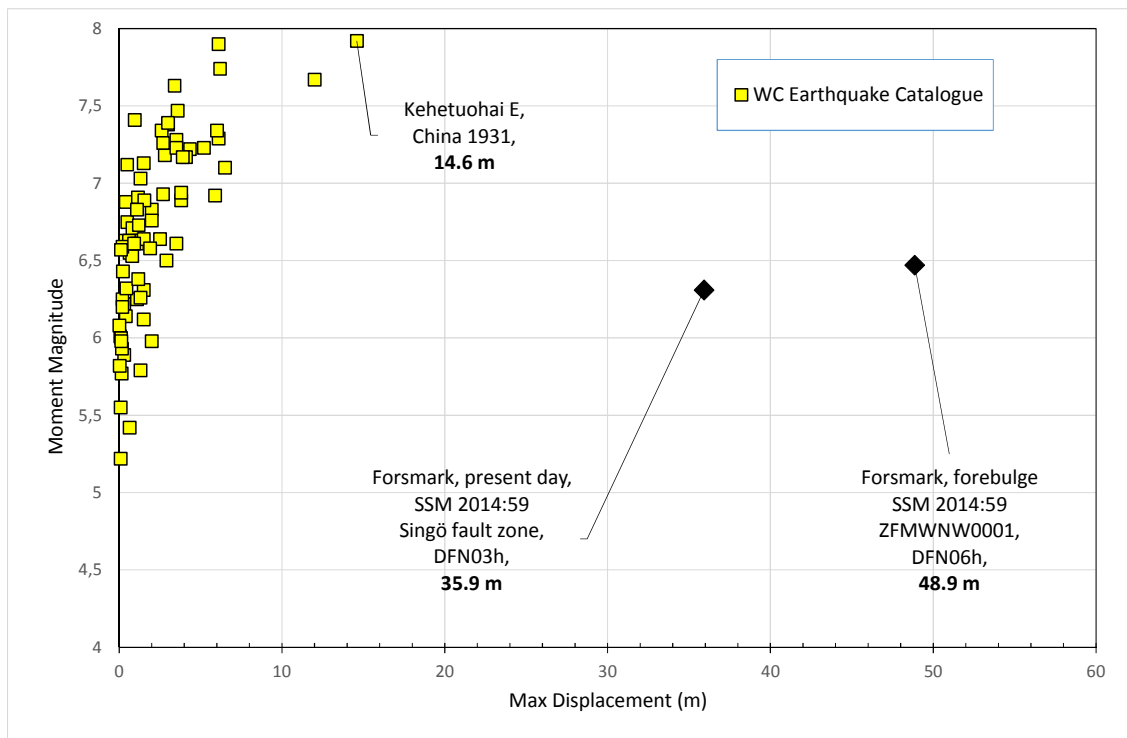


Figure 3-11. Two of the Singö deformation zone earthquakes as modelled by Yoon et al. (2014) plotted along with the Wells and Coppersmith (1994) data. Displacements given for the Singö fault zone earthquakes are mean displacements, while the displacements given for the database earthquakes are maximum displacements.

3.3.3 Fault slip velocities

The fault slip velocity is an important parameter that contributes to determine the amplitude of the stress waves generated by the earthquake and, consequently, its dynamic impact on the surrounding host rock fractures. The 1999 Chi-Chi Taiwan earthquake (M_w 7.6) is reputed for its high slip velocities, calculated from among the highest ground velocities ever instrumentally recorded. The maximum slip velocity of the Chi-Chi earthquake was estimated to about 4.5 m/s (Ma et al. 2003). The maximum slip velocities obtained in the 2D PFC models are not specified in Yoon et al. (2014). For some of the 2D earthquakes the average velocities amount to more than 100 m/s, i.e., more than 20 times higher than the maximum slip velocity of the Chi-Chi magnitude 7.6 earthquake. This result is obviously unreasonable but is not commented or explained in Yoon et al. (2014).

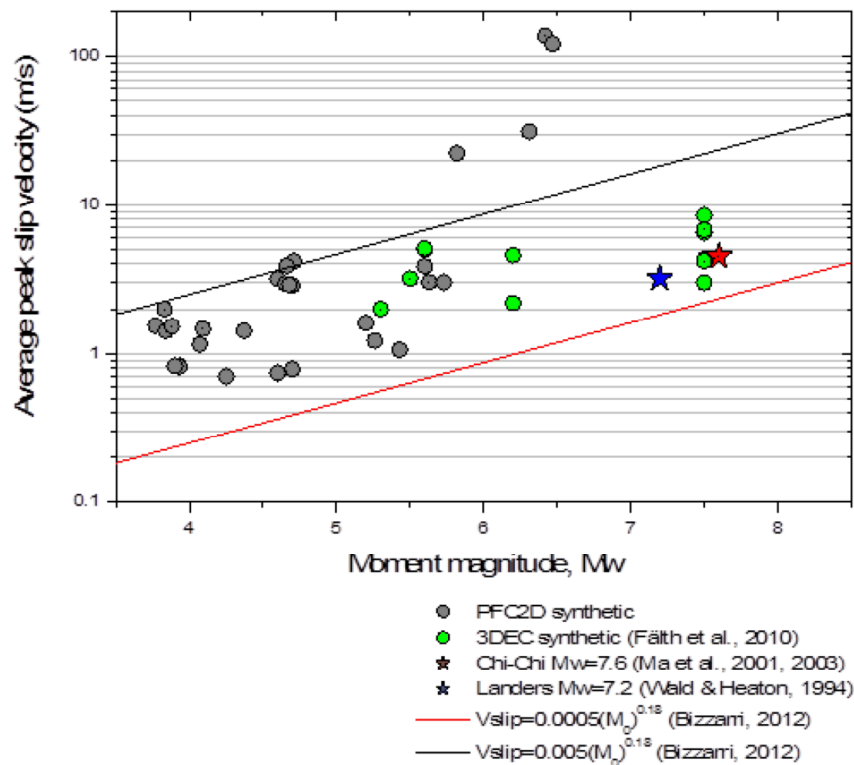


Figure 3-12. Slip velocities (Figure 99 in Yoon et al. (2014))

3.4 Possible explanations for the PFC results

In this section we bring up a few, quite specific, technical details that have to be taken into account when using PFC for performing SRM (Synthetic Rock Mass) simulations. If these aspects are not taken into account, or inadequately accounted for, the simulation results might be quite misleading.

3.4.1 Smooth-joint representation of discontinuities (faults, fractures, joints, foliation planes)

Yoon et al. (2014) states “As mentioned earlier in Sec. 4.1, a single line fracture (joint) is represented as a collection of small length segments consisting of smooth joint elements. This is illustrated in Figure 1. Such representation of a fracture might be more reasonable than straight lines as fractures in nature do not show perfectly planar structures and, irrespective of the surface roughness observed in laboratory, fractures may be undulated or stepped at large scale (Fälth et al., 2010).”

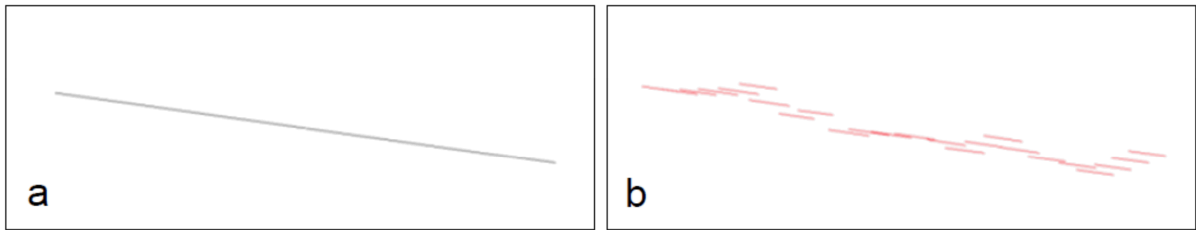


Figure 3-13. Conversion of (a) a single planar joint to (b) a collection of smooth joints (from Yoon et al. 2014, Figure 17).

We recall that the discontinuity planes represented in PFC are collections of smooth joint elements between particles that lie at both sides of the defined joint plane. The joint contact is described as smooth because particle pairs joined by a smooth-joint contact may overlap and “slide” past each other, instead of being forced to move around one another (Figure 3-14). The effective joint geometry of a single smooth joint consists of two initially coincident planar surfaces (Mas Ivars et al. 2008; Itasca 2015).

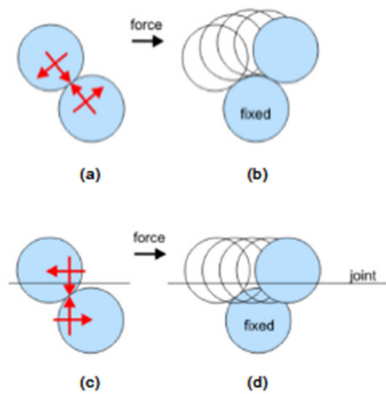


Figure 3-14. (a) Standard contact model (relative normal and tangential displacements with respect to contact orientation), (b) motion of upper particle with a standard contact when subjected to a lateral force, (c) smooth-joint contact model (relative normal and tangential displacements with respect to the joint orientation) and (d) motion of upper particle with a smooth-joint contact when subjected to a lateral force.

The visual roughness or waviness shown in Figure 3-13b is an artefact of the particle size. If the particle sizes are sufficiently small, the discontinuity plane will be almost planar. Depending on the particle size (quite large in this case) the plane will look quite like in Figure 3-13b or Figure 3-15. However it will, mechanically, behave exactly like the planar discontinuity in Figure 3-13a. That is, it will still behave like a single plane because the particles that share a smooth joint contact are infinitely soft, in order to be able to pass through each other.

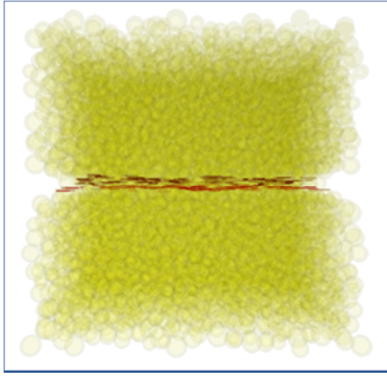


Figure 3-15. Location of smooth-joint contacts when inserting a single horizontal discontinuity in particle assembly in PFC3D.

Yoon et al. (2014) do not explain how the discontinuities have been inserted. If each one of the discontinuities has been inserted as a single plane (i.e. with dip angle, centre coordinates and radius) then each of the discontinuities will behave like a planar structure regardless of the visual roughness defined by the smooth-joint contacts. If the intention is to have discontinuity splays then several smooth joint planes need to be defined, each one having a different centre and /or dip angle.

3.4.2 Calibration of smooth joint mechanical properties

All the area dependent micro-properties (i.e. K_n , K_s , cohesion and tensile strength) of each smooth joint contact, that for part of a smooth joint plane, have to be calibrated in order to reproduce the desired macro-property at the discontinuity plane scale. This is because a discontinuity plane in PFC is formed of a number of smooth-joint contacts along the plane. These smooth joint contacts overlap each other so that the total “actual” smooth joint contact length (area in 3D) is larger than the “theoretical” discontinuity length. This discrepancy in length depends on the particle size ratio (i.e. maximum vs minimum particle size) and the chosen particle size distribution.

In Table 4 of Yoon et al. (2014) it is indicated that the K_n has been adjusted according to the average particle diameter in the model. However, the calibration must consider the number of particles, i.e. the number of smooth joint contacts, contained in the discontinuity plane. There is also a need to calibrate K_s , cohesion and tensile strength, because they also correlate to the fracture length (or area in 3D).

A detailed explanation follows for PFC3D from Mas Ivars and Bouzeran (2013), also concluded in Vallejos et al. (2013):

First, we define two types of discontinuity area:

- The “Theoretical discontinuity area”, $Area_{th}$: the discontinuity geometrical area in the SRM specimen.
- The “Real discontinuity area”, $Area_{real}$: the sum of local area of the n smooth-joint contacts composing the discontinuity plane.

$$Area_{real} = \sum_1^n SJ_area_{micro}(j)$$

$$Area_{th} \begin{cases} Area_{th,cy} = (Radius_{macro})^2 \cdot \Pi' \\ Area_{th,sq} = L^2 \end{cases}$$

where $Radius_{macro}$ = vein radius and L = vein length.

The square area $Area_{th,sq}$ has been applied to square discontinuity shape used for the direct shear tests; the cylindrical area $Area_{th,cy}$ has been applied to circular vein shape used for the direct tensile and UCS tests. These tests are used during the calibration process.

In PFC3D, discontinuity planes are formed of numerous smooth joint contacts which areas overlap each other (see Figure 3) so that usually $Area_{real}$ is larger than $Area_{th}$.

If we want to compare the results of tests on discontinuities from the lab to the results from SRM simulations then, the macro-stress in the discontinuities has to be computed by dividing the sum of forces in the discontinuity by the theoretical discontinuity area. If the vein plane is composed by n smooth joint contacts, it means:

$$\sigma_{ii,MACRO} = \frac{\left[\sum_1^n F_{i,micro}(j) \right]}{Area_{th}}$$

The macro-stiffness corresponds to the average of the micro-stiffness of the smooth joint contacts forming the discontinuity plane. It is computed by dividing the average micro-stress (normal or shear) by the average displacement, as follows:

$$K_i = \frac{\sigma_{ii,MACRO}}{Disp_i}$$

Where:

$$Disp_i = \frac{\left[\sum_1^n Disp_{i,micro}(j) \right]}{n}$$

The cohesion is estimated in this project by the difference between strength peak (or strength envelop) without cohesion and with cohesion. In order to do this estimation, a series of direct shear tests at different confinement is performed, first without cohesion, and then, with cohesion.

If we consider the above definitions, and if the discontinuity behaves as it should, then the macro vein properties are equal to the micro ones when not measuring stress (friction and dilation, in degrees), the macro vein properties are equal the micro ones multiplied by the ratio $Area_{real}/Area_{th}$

when measuring stress (normal and shear stiffness, cohesion and tensile strength respectively expressed in Pa/m, Pa and Pa).

Based on this, an extensive number of UCS, direct tension and direct shear simulations on PFC3D SRM samples with particle size uniform distribution and particle size ratio of 1.66 were performed.

From those simulations the smooth joint area ratio ($A_{ratio} = \text{Area}_{real} / \text{Area}_{th}$) was computed for several particle resolutions (i.e. number of particles along the side length of the discontinuity) and several particle generation seed numbers. Figure 3-16 shows the results.

It can be observed that:

- The Area ratio depends on the particle generation seed number and vein resolution (number of particles along the discontinuity diameter/length).
- The smaller the resolution, the higher the variability.
- The Area ratio lies between 1.32 (res=3) and 2.25 (res>16).
- The ratio increases with resolution following a clear tendency.

Figure 3-17 shows the exponential fit of the results. The expression is as follows:

$$Area_{ratio} = -1.122 \cdot e^{-\frac{x}{4.184}} + 2.134$$

where x is the discontinuity resolution.

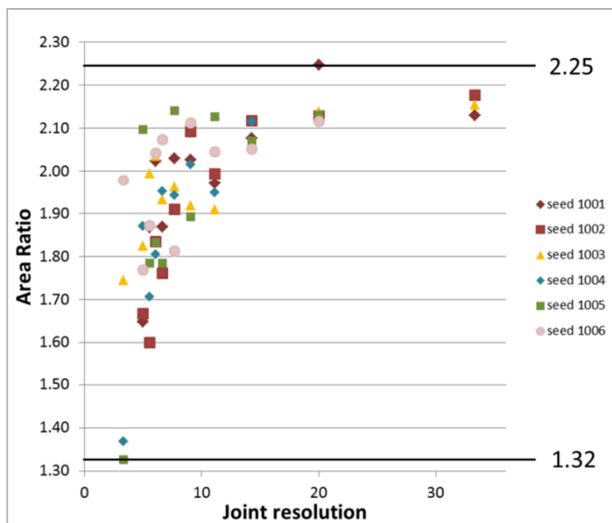


Figure 3-16. A_{ratio} computation vs discontinuity resolution and seed number.

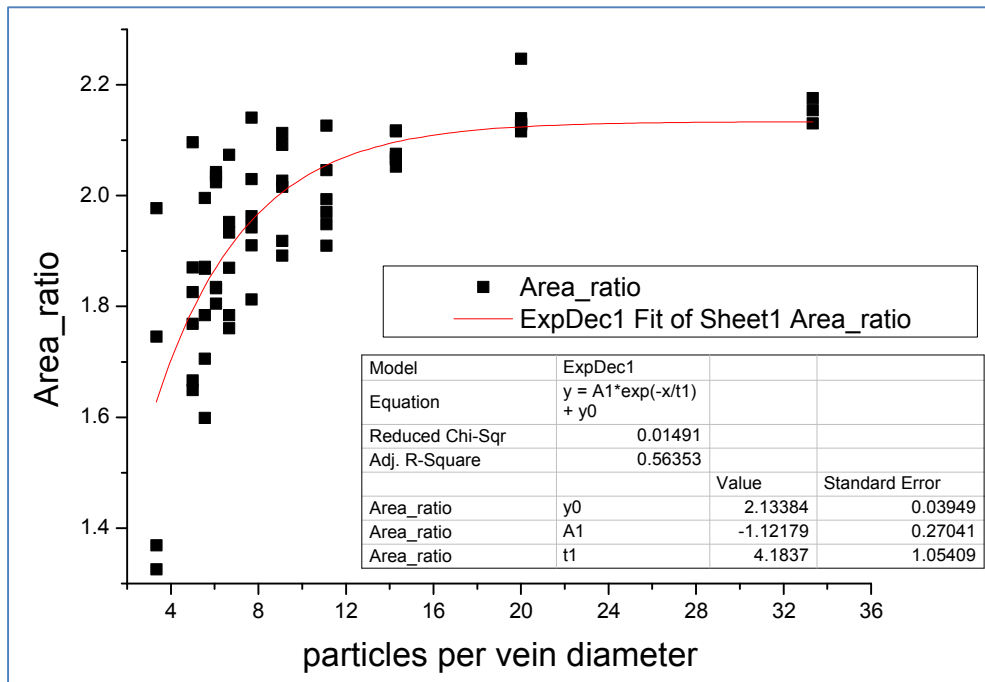


Figure 3-17. A_{ratio} computation vs discontinuity resolution: exponential fit.

Table 3-1 presents the summary of the calibration procedure in PFC3D. A similar process should be followed in 2D.

Table 3-1. Error rate in the estimation of the macro/micro relation based on the A_{ratio} concept.

	Estimation of the macro value	Error rate
Normal Stiffness	Micro value $\times A_{ratio}$	<1%
Shear stiffness	Micro value $\times A_{ratio}$	<1%
Tensile strength	Micro value $\times A_{ratio}$	From 0 to 10%
Friction angle	Micro value	From 0 to 5%
Cohesion	Micro value $\times A_{ratio}$	From 0 to 10%
Dilation	Micro value	From 0 to 8%

In conclusion, Yoon et al. (2014) indicate that the induced displacement is uncorrelated to target fracture size. This counterintuitive conclusion can be explained by a too low particle resolution along the shorter target fractures, which would make them softer and weaker, i.e. lower macro K_s and cohesion, in comparison to larger target fractures in which the resolution would be larger. Yoon et al. (2014) do not comment on the average particle diameter or the particle size ratio used in the simulations so this possible simulation flaw cannot be assessed by us. To avoid such particle resolution effect, a minimum of 12-20 particles along the shorter discontinuity in the model is required (see Figure 3-17). Otherwise, each simulated target fracture should be given its own micro-properties in relation to its own particle resolution.

3.4.3 Smooth joint based DFN (effect of discontinuity intersections and discontinuity terminations)

During the presentation of the work reported in Yoon et al. (2014) at the workshop in Eurajoki, Finland (November 2015), a few examples were shown in which the smooth joint behaviour was tested. The results showed a few spikes that Dr Yoon had difficulties explaining. We recall the origin of those numerical spikes by quoting Mas Ivars et al. (2011) (with figure numbers altered):

“Since its appearance a few decades ago, discrete fracture network (DFN) simulation is considered the most logical choice to explicitly represent the structure of the in situ joint fabric. Discrete fracture networks can be generated by external software from the measured in situ joint data coming from sources like borehole logging, tunnel and outcrop scanline, or window mapping, and then imported into the SRM samples to represent the joint network. In this manner, the rock block structure can be represented explicitly in the SRM samples. In cases where two or more joints intersect at a single contact, the properties and the orientation of only one of the joints (the first joint to be inserted) are assigned to the single smooth-joint contact model, effectively introducing a large asperity on the remaining joint, or joints, that is/are controlled by the particle size. Asperities at joint intersections have an infinite strength and a size that is a function of particle size. The shear strength behaviour of joints with asperities needs further research and development.

Joint termination, joint intersection, and joint hierarchy must also be considered when constructing a DFN and embedding it within an SRM sample. Joints are created by specific stress mechanisms associated with geological events. These geological events generate sets of joints in different directions at different times. In nature, pre-existing nearby joints can modify the sizes and orientations of later joints. Structural geologists study the cross-cutting relations between different joint sets in order to determine their relative age. A variety of rules have been established to help determine the relative age of joints. Early joints tend to be long, relatively continuous, and infilled with vein material, whereas later joints are barren, abut against earlier ones, and are consequently shorter (Figure 3-18a-c from Harries (2001)). In cases where a joint hierarchy is evident, this can be accounted for in the order of insertion of joints in the SRM sample. The first joint (or joint set) inserted will always be “continuous” in its entirety becoming dominant, while subsequent joints (or joint sets) intersecting the first one will have large asperities in the shared contacts at the intersections and thus be “discontinuous”. In some sense, this is equivalent to Figure 3-18a and Figure 3-18c in which the secondary joint set is “discontinuous”. However, in the SRM sample the behaviour in the intersection will be controlled by the size of the asperity (i.e. the particle size). Joints terminating in other joints will also have a large asperity of infinite strength in the shared contact, which size will depend on the model particle size. If no data on joint hierarchy is available or there is no evidence of joint hierarchy, then the choice is made randomly, effectively mimicking a random joint hierarchy.”

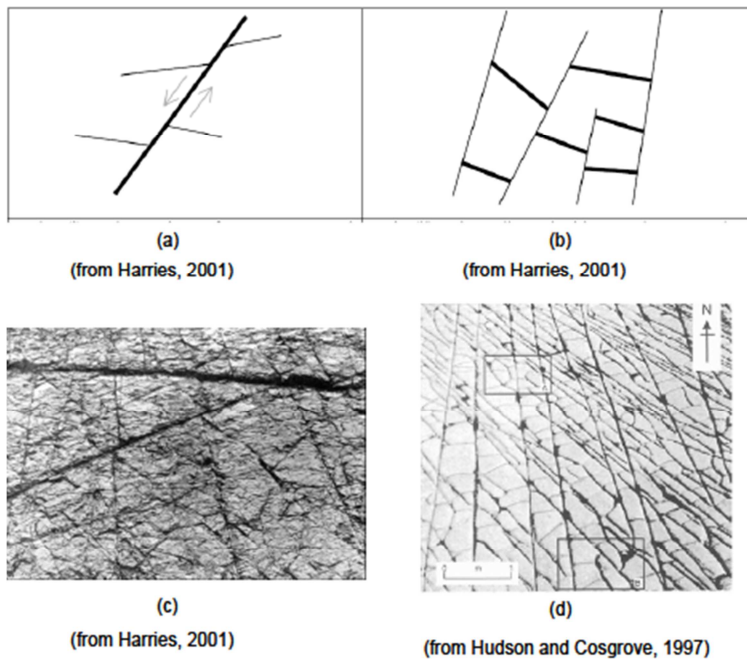


Figure 3-18. Joint interaction age determination rules (Harries 2001): (a) where shear fractures cut and displace another discontinuity set, the discontinuity set that has been displaced is obviously the older fracture set; and (b) where discontinuities terminate on other discontinuities, the discontinuity set that terminates is the younger set and the discontinuity set that stops the other discontinuity from propagating is the older discontinuity set. (c) Fracture network of the Holderbank quarry, and (d) fracture patterns in a limestone pavement at Lilstock, North Somerset, SW England. The older fracture sets are the most continuous and, as the sets become progressively younger, they become less continuous and less well oriented (from Hudson and Cosgrove 1997).

A clear example of the influence of the insertion order of smooth joint planes is presented in the following paragraphs and Figures 9-11 from Mas Ivars (2010).

“The SRM approach has been used to explore the effect of joint hierarchy in rock mass behavior in a study performed for Bing-ham Canyon mine. In this case study, the rock mass exhibited a sub-horizontal bedded structure combined with a couple of sub-vertical joint sets (see Figure 3-19).

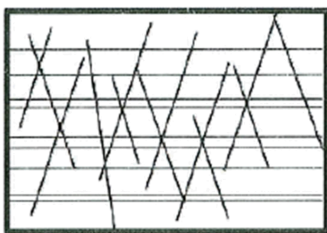


Figure 3-19. Scheme showing the sub-horizontal bedding structure and the two sub-vertical joint sets of the Quartzite unit at Bingham Canyon (Bingham Canyon study case). (Figure 9 in Mas Ivars (2010).)

There was no information on the hierarchical order of the two sub-vertical joint sets so it was decided to build and test two SRM samples (hybrid B and hybrid B2) each of them with a different sub-vertical joint hierarchy (Figure 3-20). In both cases, in order to make the sub-horizontal bedding planes fully persistent they were inserted first. In the hybrid B model joint set 1 was inserted in second place (the next more continuous joint set) and joint set 2 was last to be inserted (the least continuous). In the

hybrid B2 model the second most continuous was joint set 2 (inserted in second place) and the least continuous was joint set 1 (inserted in last place).

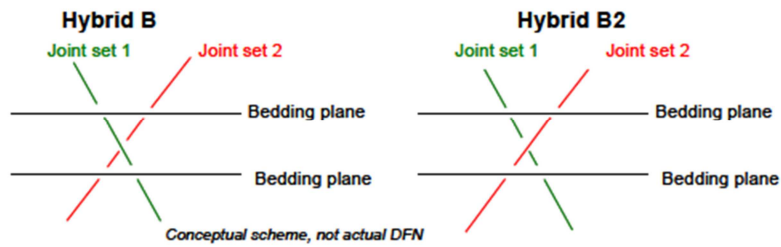


Figure 3-20. Scheme showing the two hierarchical conceptual models of the joint network of the quartzite unit at Bingham Canyon mine. (Figure 10 in Mas Ivars (2010).)

Both joint sets had the same mechanical properties. The results of a simulated UCS test on a hybrid B SRM sample and a hybrid B2 SRM sample are shown in Figure 3-21.

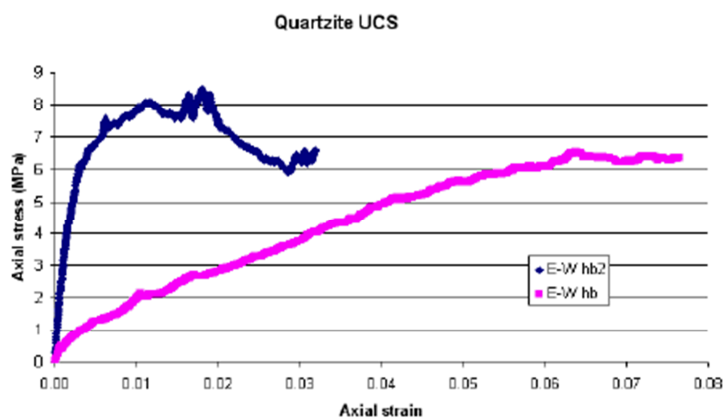


Figure 3-21. Simulated axial stress vs. axial strain response during a UCS test per-formed on SRM samples representing Quartzite from Bingham Canyon mine with hybrid B joint network and hybrid B2 joint network (Bingham Canyon study case). (Figure 11 in Mas Ivars (2010).)

The SRM model with hybrid B2 joint hierarchy (joint set 2 relatively more continuous than joint set 1) is stiffer, stronger and more brittle than the one with hybrid B joint hierarchy. Joint set 1 is much more numerous than joint set 2 in the DFN. Joint set 1 being broken in small joint segments with asperities (hybrid B2 joint hierarchy) can cause increase in strength, brittleness, and stiffness.”

Yoon et al. (2014) provide no information on how joint hierarchy was addressed with regards to smooth joint plane insertion order, i.e. to the simulation sequence. As we have shown above, the simulation sequence can have a dramatic effect on the results (Figure 3-21), everything else held equal. The spurious “spikes” shown at the seminar at Eurajoki (but not reported in Yoon et al. (2014)) can thus have its cause in the simulation sequence. The infinitely strong asperities in intersections between smooth joint planes can be minimized by using higher particle resolution. However, the effect is very difficult to quantify and this should be carefully considered when setting up the problem and analysing the results of the modelling.

3.4.4 Type of bond used vs. rock behaviour modelling and rock damage estimation

We cannot find any information in Yoon et al. (2014) regarding the type of bonding material (i.e. parallel bond or flat-joint) used for the simulations.

The parallel bond used in combination with a uniform particle size distribution with particle size ratio around 1.66 cannot capture the friction angle nor the UCS/tensile strength ratio of brittle rock (e.g. Potyondy and Cundall 2004). There are different solutions for this including particle clusters and clumps (Potyondy and Cundall 2004; Cho et al. 2007), by varying the porosity and the proportion of initial bonded contacts in the assembly (Schöpfer et al. 2009), and recently the flat-joint model (Potyondy 2012).

If the parallel bond has been used, due to the high confinement environment at depth in the Forsmark area, the rock damage simulated (i.e. intact rock bond breakage) may be misleading.

3.5 Final remarks

3.5.1 General

There are many problematic issues to discuss and question in the report by Yoon et al. (2014).

One issue is the glacial periods selected for analysis of the seismic risk for the Forsmark repository. Out of 38 simulations, 11 regard the time of maximum ice load, i.e., a period of increased stability for deformation zones of all orientations. The stability increase is confirmed by comparing the CFS estimates in Figure 28 of Yoon et al. (2014) (present day) and Figure 30 (glacial maximum). The stability increases (for all zones considered) by between 5 and 8 MPa, taking the CFS value as stability measure. This is in agreement with results presented in (Hökmark and Fälth 2014) for a number of differently oriented Olkiluoto deformation zones: all deformation zones, gently dipping ones as well as steeply dipping ones, are stabilized during the glacial maximum. Eight models out of 38 in Yoon et al. (2014) regard the forebulge. Comparing Figures 28 and 29 in Yoon et al. (2014), it appears that the forebulge stability is almost identical with the present-day stability in their study. Only five out of 38 models regard the endglacial phase, during which the seismicity (in contrast to the forebulge and the glacial maximum) in the Baltic Shield should be expected to increase. No estimates of the end-glacial stability are, however, shown in the Yoon et al. (2014). The gently dipping ZFMA2 deformation zone, which is the one considered in the end-glacial models in Yoon et al. (2014), is not included in the stability estimates shown in Figures 28-30. In Fälth and Hökmark (2013) it is shown that ZFMA2 is not only close to the stability limit under present day conditions; it is also significantly destabilized under end-glacial conditions, which supports the choice of ZFMA2 as a relevant case for the endglacial models in Yoon et al. (2014). The results are, however, not credible: At the time of the stable glacial maximum, the PFC2D model produces a ZFMA2 earthquake of magnitude 5.9 (Yoon et al. 2014, table 12), while the corresponding earthquake occurring at the time of ice retreat, when ZFMA2 would be considerably destabilized, is of magnitude 5.73. Figure 3-22 shows that even gently dipping deformation zones, such as ZFMA2 would be stabilized rather than destabilized at the time of glacial maximum. This indicates that there is little or no physically relevant coupling between the input assumptions and the results (larger ZFMA2 earthquakes at time of glacial maximum than at time of

ice retreat). If this is a consequence of arbitrary implemented models of rupture initiation and propagation (e.g. “powered shear force”), numerical errors, 2D-effects or combinations of these problems is not possible to determine. No comments on this are made in Yoon et al. (2014).

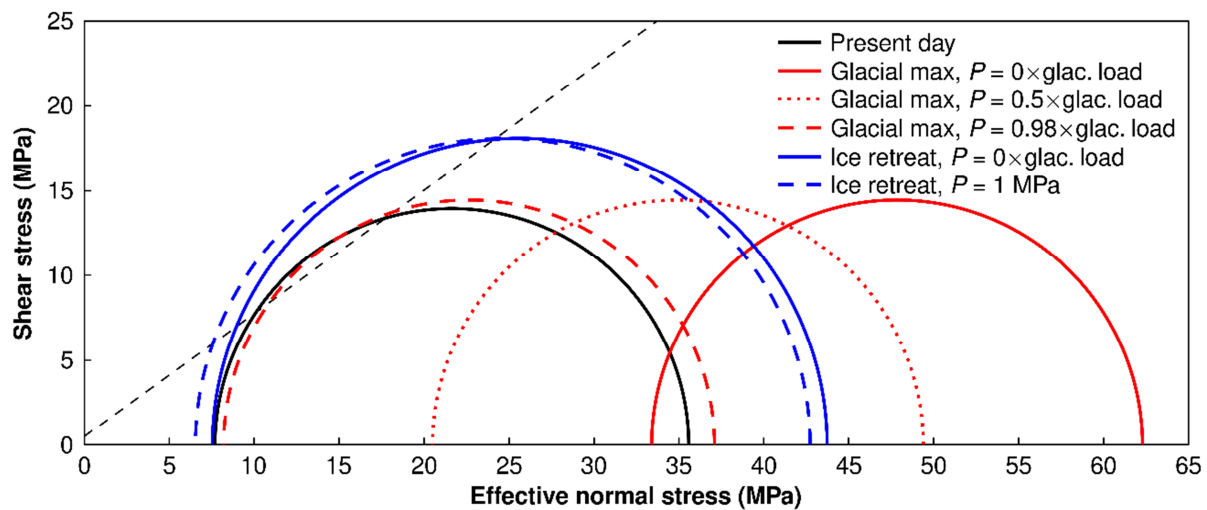


Figure 3-22. Mohr circle representation of Forsmark stress field in σ_H - σ_v plane during different glacial phases. Glacial stresses are from (Lund et al., 2009). Full lines correspond to a hydrostatic pore pressure. Dashed and dotted lines correspond to different excess pore pressure assumptions. The failure envelope ($\phi = 36^\circ$, $c = 0.5$ MPa) is plotted for reference only. Compared to present day conditions, even optimally oriented deformation zones would not be destabilized during the glacial maximum, even if the most extreme pore pressure assumption is made. At the time of ice retreat, on the contrary, there is a significant destabilization of gently dipping zones even without any excess pore pressure. In addition, the driving shear stresses are considerably higher at the time of ice retreat than during the glacial maximum. Note that no statement of any pore pressure assumptions are made in the SSM report.

Another issue is the reasons given for using the PFC2D code: For instance the possibility to capture inelastic processes such as fracture growth and fracture coalescence. Yet there are no indications, anywhere in the report, of the actual impact of these processes on the results.

It should also be noted that a previous report included in SSM’s review of SKB’s licence application (Backers et al. 2014), has commented as follows on the relevance of the PFC2D code as a tool for this type of simulations: “Each parameter in the code has to be tuned, and the parameters mostly lack of physical meaning. Hence, the tuning has to be performed for each specific case to the results of a physical experiment post hum, ergo. Forward modelling is not physically based and hence, in the Authors’ opinion, not suitable for the predictive simulation of DFN behaviour.”

Additional issues would, for instance, be: why are not pore pressures mentioned? Are they not considered at all, or implicitly accounted for by tuning frictional strength parameters? In all 3DEC models referred to in previous sections, the pore pressure, which is an important target fracture strength parameter, is explicitly included. In the end-glacial 3DEC models the fracture pore pressures was increased by one MPa to account for possible residual pressures. Are the model boundaries in Yoon et al. (2014) located sufficiently far from the rupturing faults? The viscous boundaries designed to eliminate irrelevant wave reflections may not be sufficient; the boundaries must also allow for quasi-static stress redistribution effects to be correctly captured.

In addition to these general comments, the remarks made in the previous subsections are summarized below.

3.5.2 Two dimensional model approach

The use of two-dimensional models is not adequate for handling the type of problems addressed in Yoon et al. (2014):

- Fracture networks in crystalline rocks, such as that of the Forsmark site, contain fractures of different orientations and sizes and cannot be adequately represented in a 2D model. In 2D models of fractured media, all fractures are, by construction, oriented perpendicular to the modelling plane and extend infinitely in the out-of-plane direction. The slip of individual 3D fractures caused by loading/unloading of the rock mass and the effects of the associated stress release and stress redistribution cannot be correctly captured quantitatively. Corresponding effects of multiple interacting 3D fractures are even more sensitive to the actual 3D geometry (cf. coalescence example in Figure 3-1). It has long been recognized by SKB that the three-dimensional fracture geometry is a first order effect that must be considered in numerical analyses of fractured crystalline rock masses, subjected to loads that potentially could generate extensive inelastic fracture shear displacement. This has necessitated the use of 3D codes like Poly3d and 3DEC in most SKB work on the mechanical and thermomechanical behaviour of the repository rock mass.
- For the thermo-mechanical problems addressed in Yoon et al. (2014), the three-dimensional fracture geometry is not the only reason why 2D models are inadequate:
 - Neither the effects of the increase of the horizontal background stresses with depth, nor the effects of the very significant variation of the thermal load with depth can be captured, even approximately, in the horizontal sections analysed in Yoon et al. (2014).
 - Neither plane stress nor plane strain conditions apply in these sections. Note that the flexure of the rock mass between the repository horizon and the ground surface following the thermal expansion will result in differences in vertical stress as well as in vertical strain between heated and non-heated parts of the repository footprint. This (which cannot be captured in the 2D models used by Yoon et al. (2014)) is one of the reasons why the most unstable fractures (i.e., the gently dipping ones) located within the deposition areas tend to be more stable, and slip less, than corresponding fractures located between deposition areas or just outside the repository footprint (cf. Figure 3-2). This is lucidly verified by 3D modelling results in (Hökmark et al. 2010). Yet, in Yoon et al. (2014) it is stated that fracture shear displacements are larger in the central parts than in the “outskirts” of the deposition areas.
 - In 3D models of the thermomechanical evolution of the repository host rock (Hökmark et al. 2010), the horizontal thermal stresses (at the depth of the repository) are found to amount to around five MPa after 5 years and to more than 10 MPa 50 years after deposition. In Yoon et al. (2014) it is suggested that shear displacements along vertical fractures, triggered by four microquakes occurring within the repository footprint 25 years after deposition, would result in stress release effects sufficient to eliminate these high thermal horizontal stresses completely.

- The thermal PFC modelling does not cover more than the first 50 years after deposition. There are however, already after 50 years, differences between the temperatures obtained within the repository footprint in Yoon et al. (2014) and corresponding temperatures obtained in 3D models assuming the repository layout.
- Stress waves and stress redistribution effects are 3-dimensional by nature. There is however no comments on, for instance, frequencies, wavelengths or peak ground accelerations that could be used to explore how and to what extent the 2D approach has impacted on the results.

Considering the points above, the errors associated with the 2D approach appear to be serious enough to question the relevance of the results in Yoon et al. (2014), and, consequently, the conclusions based on these results.

3.5.3 Handling of “Outliers”

Some results are classified as outliers. This seems to be done without any coupling to outliers in the statistical input. The handling of numerical errors as “outliers” appears casual and arbitrary:

- The largest and potentially most critical displacements are disregarded as “outliers” without checking whether or not these displacements actually are results of numerical disturbances. In box-whisker diagrams of target fracture displacements, the arbitrary division of the results in size classes contributes to control which displacements should be regarded as reliable and trusted, and which should be regarded as “outliers”.
- On the level of the smooth joint displacements, divided into distance classes and presented in box-whisker diagrams, it appears that around 50% of the total slip is due to outliers. This percentage (50%) is based on one randomly picked example and is therefore an indication of order of magnitude rather than a generally valid estimate of the outlier contribution.
- On the level of target fracture displacements, it appears that around 40% of the total slip is due to outliers. Again, this percentage is an approximation, based on one randomly picked example.

It is beyond the scope of this Memo to estimate to what extent the considerable outlier fractions of the total smooth-joint and target fracture displacements have contributed to control the overall behaviour of the 2D PFC fracture network.

3.5.4 Unrealistic results

Results that are obviously unrealistic and illogical are presented without comments or explanations. That the authors have not performed relevant reality checks raises the question if the modelling has been carried out without sufficient understanding of the seismological problems under study, or without serious attempts to generate credible and meaningful results.

- The results suggest that fractures of lengths between 150 m and 200 m in the horizontal section (i.e., vertical fractures) systematically slip by larger amounts than vertical fractures with lengths between 200 m and 600 m. Since one of the objectives of the study by Yoon et al. (2014) is to establish relations between fracture length and fracture shear displacement, it should be explained by which mechanical mechanisms large fractures would slip much less than

significantly smaller fractures. Especially since such a statement is in direct conflict with established theories.

- The authors present seismic displacements along the Singö fault zone that are about three times larger than the largest displacements ever observed along fault zones other than interplate subduction zones. To match the seismic displacement obtained along the 15 km long 2-dimensional Singö fault in Yoon et al. (2014), one has to compare with subduction zone events like the 2011 Tohoku magnitude 9 earthquake with a 400 km rupture length.
- The authors present shear slip velocities that are orders of magnitude higher than the maximum slip velocities suggested for large historic earthquakes, specifically reputed for high slip velocities such as the 1999 Chi-Chi, Taiwan, magnitude 7.6 earthquake (Ma et al. 2003).

4 Conclusions

As demonstrated and discussed in the previous chapter, there is a range of issues regarding the approaches and the results in Yoon et al. (2014) that, according to our view, render the suggestions and recommendation based directly on results presented in that report highly questionable.

Some of the recommendations are judged to be relevant, regardless of the PFC2D results. Analysing models with interacting neighbouring deformation zones, for instance, is a natural extension of the modelling efforts. It may also be necessary to ensure, specifically, that deformation zones with trace lengths smaller than 3 km will not require any respect distances. These issues are currently being addressed using the 3DEC modelling approach.

We should also point out that we have no objections regarding the Synthetic Rock Mass approach in general or the PFC code in particular. However, to arrive at credible quantitative stress and slip estimates, it is essential that modelling of systems with 3-dimensional fracture networks, complicated stress gradients and seismic sources are modelled in three dimensions. It is also necessary to make systematic reality checks and to ensure that couplings between input assumptions and modelling results are logical and understandable.

5 References

- Backers T, Meier T, Gipper P, Stephansson O, 2014.** Rock Mechanics – Assessing probability and extent of blind faults and fault-end growth around the KBS-3 repository at Forsmark. Technical Note 2014:58, ISSN: 2000-0456, Swedish Radiation Safety Authority.
- Cho N, Martin C D, Sego D C, 2007.** A clumped particle model for rock. International Journal of Rock Mechanics and Mining Sciences. Volume 44, issue 7, p. 997-1010
- Claesson J, Probert T, 1996.** Temperature field due to time-dependent heat sources in a large rectangular grid - Derivation of analytical solution. SKB TR 96-12, Svensk Kärnbränslehantering AB.
- Eshelby J, 1957.** The determination of the elastic field of an elliptical inclusion and related problems. Vol. A241. London: Proc. Roy. Soc.
- Fälth B, 2015.** Simulating Earthquake rupture and off-fault fracture response. Fil Lic thesis, Jan 16, 2015. Institution of Geosciences, Uppsala University.
- Fälth B, Hökmark H, 2006a.** Mechanical and thermo-mechanical discrete fracture near-field analyses based on preliminary data from the Forsmark, Simpevarp and Laxemar sites. SKB R-06-89, Svensk Kärnbränslehantering AB.
- Fälth B, Hökmark H, 2006b.** Seismically induced slip on rock fractures. Results from dynamic discrete fracture modeling. SKB R-06-48, Svensk Kärnbränslehantering AB.
- Fälth B, Hökmark H, 2011.** Modelling end-glacial earthquakes at Olkiluoto. Posiva Working Report 2011-13, Posiva Oy.
- Fälth B, Hökmark H, 2012.** Modelling end-glacial earthquakes at Olkiluoto. Expansion of the 2010 study. Posiva Working Report 2012-08, Posiva Oy Finland.
- Fälth B, Hökmark H, 2013.** Termiskt inducerade skalv. Svensk Kärnbränslehantering AB, Stockholm, Sweden. Document ID 1403906 Version 1.0, 2013-10-01.
- Fälth B, Hökmark H, 2015.** Effects of Hypothetical Large Earthquakes on Repository Host Rock Fractures., Posiva Working Report. 2015-18, POSIVA OY.
- Fälth B, Hökmark H, Lund B, 2015a. Submitted.** Simulation of co-seismic secondary fracture displacements at the proposed nuclear waste repository site in Forsmark: The effect of varying rupture scenarios. . International Journal of Rock Mechanics and Mining Sciences.
- Fälth B, Hökmark H, Lund B, Mai P M, Roberts R, Munier R, 2015b.** Simulating Earthquake Rupture and Off-Fault Fracture Response: Application to the Safety Assessment of the Swedish Nuclear Waste Repository. Bulletin of the Seismological Society of America. Volume 105, issue 1, p. 134–151. doi:10.1785/0120140090

- Fälth B, Hökmark H, Munier R, 2007.** Seismically Induced Shear Displacements in Repository Host Rock Fractures. Proceedings of 9th Canadian conference on Earthquake Engineering, Ottawa, Canada, June 26-29, 2007.
- Fälth B, Hökmark H, Munier R, 2008.** Seismically induced slip on rock fractures – expanded study with particular account of large earthquakes. Proceedings of 42nd U.S. Rock Mechanics Symposium, San Fransisco 2008, June 29 - July 2, 2008.
- Fälth B, Hökmark H, Munier R, 2010.** Effects of large earthquakes on a KBS-3 repository. Evaluation of modelling results and their implications for layout and design. Updated 2011-10. SKB TR-08-11, Svensk Kärnbränslehantering AB.
- Harries N J, 2001.** Rock mass characterisation for cave mine engineering. PhD thesis University of Queensland, Brisbane, Australia.
- Hudson J A, Cosgrove J W, 1997.** Integrated structural geology and engineering rock mechanics approach to site characterization. International Journal of Rock Mechanics and Mining Sciences. Volume 34, issue 3
- Hökmark H, Fälth B, 2014.** Approach to Assessing the Stability of Olkiluoto Deformation Zones During a Glacial Cycle. Workreport 2013-37, Posiva, Helsinki.
- Hökmark H, Lönngqvist M, Fälth B, 2010.** THM-issues in repository rock. Thermal, mechanical, thermo-mechanical and hydro-mechanical evolution of the rock at the Forsmark and Laxemar sites. SKB TR-10-23, Svensk Kärnbränslehantering AB.
- ITASCA, 2013.** 3DEC, 3 Dimensional Distinct Element Code, Users manual. Version: 4.1. ITASCA, 111 Third Avenue South, Suite 450, Minneapolis, MN 55401, USA.
- Itasca, 2015.** PFCSuite. ITASCA, 111 Third Avenue South, Suite 450, Minneapolis, MN 55401, USA.
- La Pointe P, Wallmann P, Thomas A, Follin S, 1997.** A methodology to estimate earthquake effects on fractures intersecting canister holes. SKB TR 97-07, Svensk Kärnbränslehantering AB.
- Lee S J, Huang B S, Ando M, Chiu H C, Wang J H, 2011.** Evidence of large scale repeating slip during the 2011 Tohoku-Oki earthquake. Geophysical Research Letters. Volume 38, issue 19
- Leonard M, 2010.** Earthquake Fault Scaling: Self-Consistent Relating of Rupture Length, Width, Average Displacement, and Moment Release. Bulletin of the Seismological Society of America. Volume 100, issue 5A, p. 1971-1988
- Lund B, Schmidt P, Hieronymus C, 2009.** Stress evolution and fault stability during the Weichselian glacial cycle. SKB TR-09-15, Svensk Kärnbränslehantering AB.
- Lönngqvist M, Hökmark H, 2013.** Thermal and thermo-mechanical evolution of the Äspö Prototype Repository rock mass. Modelling and assessment of sensors data undertaken in connection with the dismantling of the outer section. R-13-10, Svensk Kärnbränslehantering AB.

- Lönnqvist M, Hökmark H, 2015.** Assessment of method to model slip of isolated, non-planar fractures using 3DEC. Proceedings of 13th International Symposium on Rock Mechanics (ISRM Congress 2015), Canada, May 10-13, 2015, 2015.
- Ma K-F, Brodsky E E, Mori J, Ji C, Song T-R A, Kanamori H, 2003.** Evidence for fault lubrication during the 1999 Chi-chi, Taiwan, earthquake (M_w 7.6). Geophysical Research Letters. Volume 30, issue 5, p. 4. doi:10.1029/2002GL015380
- Martin C D, 2007.** Quantifying in situ stress magnitudes and orientations for Forsmark. Forsmark stage 2.2. SKB R-07-26, Svensk Kärnbränslehantering AB.
- Mas Ivars D, 2010.** Bonded Particle Model for Jointed Rock Mass. PhD thesis Royal Institute of Technology, KTH, Stockholm, Sweden.
- Mas Ivars D, Bouzeran L, 2013.** Final report on Synthetic Rock Mass (SRM) Fragmentation Analysis – Appendix 2 – Vein Calibration. . El Teniente, Codelco.
- Mas Ivars D, Pierce M E, Darcel C, Reyes-Montes J, Potyondy D O, Young R P, Cundall P A, 2011.** The synthetic rock mass approach for jointed rock mass modelling. International Journal of Rock Mechanics and Mining Sciences. Volume 48, issue 2, p. 219-244
- Mas Ivars D, Potyondy D O, Pierce M, Cundall P A, 2008.** The Smooth-Joint Contact Model. Proceedings of 8th World Congress on Computational Mechanics (WCCM8), Venice, Italy, 2008.
- Munier R, Stenberg L, Stanfors R, Milnes A G, Hermanson J, Triumf C-A, 2003.** Geological Site Descriptive Model. A strategy for the model development during site investigations. SKB R-03-07, Svensk Kärnbränslehantering AB.
- Ofoegbu G I, Smart K J, 2012.** Shear movement of nearfield rock due to large earthquakes. Technical Note 2012:57, ISSN: 2000-0456, Swedish Radiation Safety Authority.
- Potyondy D, 2012.** A flat-jointed bonded-particle material for hard rock. Proceedings of 46th US Rock Mechanics/Geomechanics Symposium, 2012. American Rock Mechanics Association.
- Potyondy D O, Cundall P A, 2004.** A bonded-particle model for rock. International Journal of Rock Mechanics & Mining Sciences. Volume 41, p. 1329-1364
- Raiko H, Sandström R, Rydén H, Johansson M, 2010.** Design analysis report for the canister. SKB TR-10-28, Svensk Kärnbränslehantering AB.
- Schöpfer M P, Abe S, Childs C, Walsh J J, 2009.** The impact of porosity and crack density on the elasticity, strength and friction of cohesive granular materials: insights from DEM modelling. International Journal of Rock Mechanics and Mining Sciences. Volume 46, issue 2, p. 250-261
- Segedin C, 1951.** Note on a penny-shaped crack under shear. Proceedings of Mathematical Proceedings of the Cambridge Philosophical Society, 1951. Cambridge Univ Press.
- SKB, 2008.** Site description of Forsmark at completion of the site investigation phase. SDM-Site Forsmark. SKB TR-08-05, Svensk Kärnbränslehantering AB.

- Spudich P, Xu L, 2002.** Documentation of software package COMPSYN svx3.11: Programs for earthquake ground motion calculation using complete 1-D Greens functions. In Lee W H K, Kanamori H, Jennings P C, Kisslinger C (eds). International Handbook of Earthquake & Engineering Seismology: Part B Academic Press, London, United Kingdom. ISBN: 0-12-440658-0.
- SSM, 2015.** Slutförvarets initialtillstånd och genomförbarhet för uppförande och drift med avseende på långsiktig strålsäkerhet. Dokumentnr: 13-3523, Swedish Radiation Safety Authority.
- Starr A, 1928.** Slip in a crystal and rupture in a solid due to shear. Proceedings of Mathematical Proceedings of the Cambridge Philosophical Society, 1928. Cambridge Univ Press.
- Vallejos J, Brzovic A, Lopez C, Bouzeran L, Mas Ivars D, 2013.** Application of the Synthetic Rock Mass approach to characterize rock mass behavior at the El Teniente Mine, Chile. Proceedings of Proceedings of the 3rd International FLAC/DEM Symposium, Itasca Consulting Group, Hangzhou, China, 2013.
- Wells D L, Coppersmith K J, 1994.** New empirical relationships among magnitude, rupture length, rupture width, rupture area, and surface displacement. Bulletin of the Seismological Society of America. Volume 84, issue 4, p. 974-1002
- Yagi Y, Fukahata Y, 2011.** Rupture process of the 2011 Tohoku-oki earthquake and absolute elastic strain release. Geophysical Research Letters. Volume 38, issue 19
- Yoon J S, Stephansson O, Min K-B, 2014.** Relation between earthquake magnitude, fracture length and fracture shear displacement in the KBS-3 repository at Forsmark. Technical Note 2014:59, ISSN: 2000-0456, Swedish Radiation Safety Authority.